Relaxation in Rubidium-87 and the Rubidium Maser

JACQUES VANIER*
Hewlett-Packard Company, Beverly, Massachusetts
(Received 5 July 1967)

The theory of the rubidium-87 maser is described. It is shown that the maser power output is a critical function of the rubidium density, light intensity, and cavity Q. Fundamental parameters and constants of the maser are grouped together to define an oscillation parameter Γ_m' which determines the oscillation characteristics of the maser. Spin-exchange calculations in rubidium are presented. The relaxation times T_1 and T_2 due to spin-exchange interactions are related to each other, and it is shown that $T_2 = (8/5)T_1$. A method of determining the spin-exchange cross section in terms of fundamental constants and maser parameters is described. Results of experiments made to verify these calculations are given. It is found in general that the results agree with the theory, but slight discrepancies exist. Tentative explanations are given.

I. INTRODUCTION

TRANSITIONS in the ground states of hydrogen and alkali atoms have been widely used in the past to probe physical interactions in atoms. Instruments built on the basis of these hyperfine transitions have proven to be stable frequency sources and useful tools for accurate studies of phenomena such as the interaction of light with atoms,[1,2] spin-exchange interaction,[3,4] and collisions of atoms with foreign gases and surfaces.[4,5] With the advent of the optically pumped rubidium maser as an active oscillator,[6–8] it appears that these effects can be measured with a new degree of accuracy. This is due to the feasibility of obtaining large power output which makes possible the realization of large signal-to-noise ratios and the observation of the true characteristics of the atoms without degradation by receiving equipment. It follows also that the rubidium maser is one of the microwave sources which has the highest spectral purity.[9]

Very few results have been published, however, on the behavior of the rubidium maser, and its limitations are not yet completely known. In the present paper the theory of the rubidium maser is developed for continuous and pulse operation. Results of detailed calculations of spin-exchange interactions in Rb^{87} are reported. A method of measuring the rubidium spin-exchange cross section without a previous knowledge of the rubidium density is described in some detail.[10] Finally, results of experiments made on a cell-type maser are reported.

II. THEORY

The theory is divided into two parts. A first part deals with the rubidium maser under continuous and pulse operation. A second part deals with detailed calculations of spin-exchange interactions in Rb^{87}.

A. The Rubidium Maser

A schematic diagram of the rubidium maser is shown in Fig. 1. It consists essentially of a quartz cell containing nitrogen at a pressure of 11 Torr and the isotope Rb^{87}. The cell is enclosed in a high Q cavity. Light from an Rb^{87} lamp, filtered by a cell containing Rb^{85}, penetrates inside the cavity and orients the Rb^{87} atoms. The energy levels of the rubidium atom are shown in Fig. 2. The purpose of the Rb^{85} filter is to remove from the spectrum of the Rb^{87} lamp the line at the frequency corresponding to the transitions from the P state to the level $F=2$ of the ground state.[5] After the rubidium atoms have been excited to the P state, they are relaxed to both levels $F=1$ and $F=2$ of the ground state by collisions with nitrogen molecules. Because of the asymmetry in the pumping light, a net population imbalance is obtained. When enough atoms are "pumped" into the upper level $F=2$, self-sustained oscillations are observed between the $F=2, M_f=0$ and $F=1, M_f=0$ levels at a frequency of 6.835 GHz.

1. Continuous-Wave Operation

In order to obtain a mathematical closed-form solution of the operation of the maser, the following assumptions are made:

1. Reradiation is completely quenched by the nitrogen buffer gas.

2. The decay from the excited states takes place randomly with equal probability to any of the ground states.

3. In the ground state, in the absence of light, relaxation taking place through collisions produces an equilibrium situation with all atoms equally distributed among the eight Zeeman sublevels shown in Fig. 2.

4. The incident light consists of the line $P \rightarrow S$ $(F=1)$; in other words we assume an ideal Rb^{85} filter.

---

* Present address: Département du Génie Electrique, Université Laval, Ste. Foy, P. Q., Canada.

[1] C. Cohen-Tannoudji, thesis, Faculte des Sciences de l'Universite de Paris, 1962 (unpublished).

[2] J. P. Barrat and C. Cohen-Tannoudji, J. Phys. Radium **22**, 329 (1961).

[3] J. P. Wittke and R. H. Dicke, Phys. Rev. **103**, 620 (1956).

[4] H. C. Berg, Phys. Rev. **137**, A1621 (1965).

[5] P. L. Bender, E. C. Beaty, and A. R. Chi, Phys. Rev. Letters **1**, 311 (1958).

[6] P. Davidovits, Appl. Phys. Letters **5**, 15 (1964).

[7] P. Davidovits and W. A. Stern, Appl. Phys. Letters **6**, 20 (1965).

[8] P. Davidovits and R. Novick, Proc. IEEE **54**, 155 (1966).

[9] For a review of the state of the art of atomic frequency standards, the reader is referred to an article by A. O. McCoubrey, Proc. IEEE **54**, 116 (1966).

[10] J. Vanier, Phys. Rev. Letters **18**, 333 (1967).

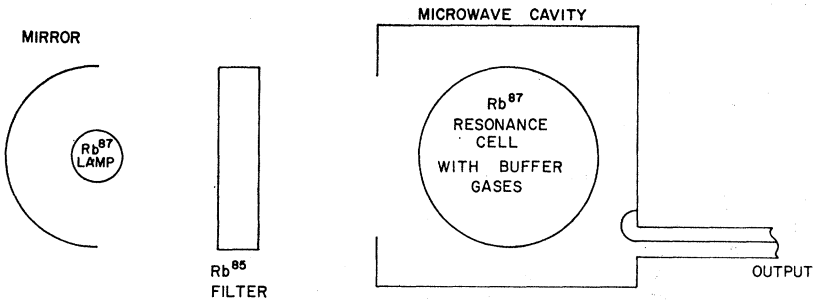

FIG. 1. Basic components of rubidium maser.

The theory thus describes the operation of an ideal maser which would operate according to these assumptions.

a. Master equations. The equilibrium density matrix ρ in the laboratory frame of reference is written for the ground state as:

$$\rho=\begin{Bmatrix}\rho_{11} & 0 & 0 & 0 & 0 & 0 & 0 & 0\\ 0 & \rho_{22} & 0 & 0 & 0 & 0 & 0 & 0\\ 0 & 0 & \rho_{33} & 0 & 0 & 0 & \rho_{37} & 0\\ 0 & 0 & 0 & \rho_{44} & 0 & 0 & 0 & 0\\ 0 & 0 & 0 & 0 & \rho_{55} & 0 & 0 & 0\\ 0 & 0 & 0 & 0 & 0 & \rho_{66} & 0 & 0\\ 0 & 0 & \rho_{73} & 0 & 0 & 0 & \rho_{77} & 0\\ 0 & 0 & 0 & 0 & 0 & 0 & 0 & \rho_{88}\end{Bmatrix}. \quad (1)$$

The hyperfine levels are numbered from high to low energy. It is assumed that the transition takes place between the field-independent levels 3 and 7. The rate of change of any element is given by

$$\frac{d\rho}{dt}=\left(\frac{d\rho}{dt}\right)_{\rm op}+\left(\frac{d\rho}{dt}\right)_{\rm rel}+\left(\frac{d\rho}{dt}\right)_{\rm rad}, \quad (2)$$

where $(d\rho/dt)_{\rm op}$ is the change with time of any element due to the pumping light; $(d\rho/dt)_{\rm rel}$ is the change with time of any element due to relaxation processes in the ground states. The processes include, for example, collisions between rubidium atoms and nitrogen molecules and rubidium-rubidium spin-exchange collisions; $(d\rho/dt)_{\rm rf}$ is the change with time caused by rf radiation.

(1) Optical pumping. The effect of the light on the density matrix elements is given by the following expressions[2]:

$$d\rho_{\mu\mu'}/dt=-A_{\mu'\mu'}[\tfrac{1}{2}\Gamma_{\mu'}-i\Delta E_{\mu'}]\rho_{\mu\mu'} -A_{\mu\mu}[\tfrac{1}{2}\Gamma_{\mu}+i\Delta E_{\mu}]\rho_{\mu\mu'}, \quad (3)$$

where $A_{\mu\mu}$ is a term representing the polarization of the light and its interaction with the atom; Γ_μ is a term proportional to the light intensity and the cross section for absorption of a photon by an atom; ΔE_μ are frequency shifts produced by the radiation field.[11] In the present case, due to assumption 4, we have

$$\Gamma_\mu=0 \quad \text{for} \quad \mu=1, 2, 3, 4, 5. \quad (4)$$

We define

$$A_{\mu\mu}\Gamma_\mu=\Gamma(z,r) \quad \text{for} \quad \mu=6, 7, 8, \quad (5)$$

$$A_{33}\Delta E_3-A_{77}\Delta E_7=\Delta\omega_l(z,r)=\text{light shift}. \quad (6)$$

In the analysis, z is the direction of the magnetic field and of incidence of the light; r is a distance in the cavity measured from the axis of symmetry. The pumping rate Γ, the density matrix element ρ, and the light shift $\Delta\omega_l$ are all functions of the distance of penetration of the light inside the maser cell. Actually, Γ can be written

$$\Gamma(z,r)=\int_0^\infty I(\nu,z,r)\sigma(\nu)d\nu, \quad (7)$$

where $I(\nu,r)$ is the light intensity at frequency ν, and position (z,r) in the maser cell, and $\sigma(\nu)$ is the cross section for absorption of a photon. Following Balling *et al.*[12] we average $\Gamma(z,r)$, $\rho(z,r)$, and $\Delta\omega_l(z,r)$ over the cell; we call them respectively Γ, ρ, and $\Delta\omega_l$; and we write

$$(d\rho_{\mu\mu}/dt)_{\rm op}=-\Gamma\rho_{\mu\mu}, \quad \mu=6, 7, 8, \quad (8)$$

$$(d\rho_{73}/dt)_{\rm op}=-\tfrac{1}{2}\Gamma\rho_{73}-i\Delta\omega_l\rho_{73}. \quad (9)$$

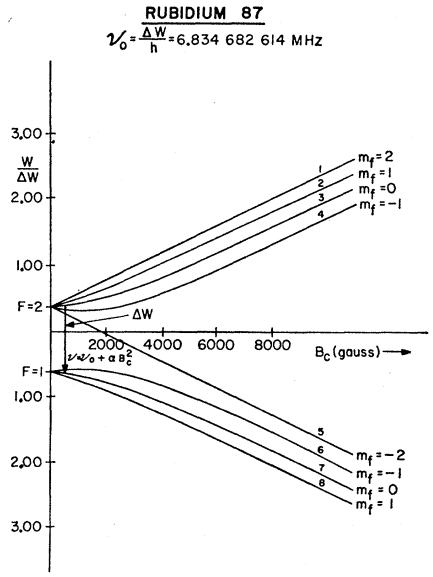

FIG. 2. Lower energy levels of a rubidum atom.

[11] In Cohen-Tannoudji's analysis, $\hbar$ is set equal to 1.

[12] L. C. Balling, R. J. Hanson, and F. M. Pipkin, Phys. Rev. 133, 607 (1964).

In this context, for a given light intensity I_0 incident on the cell, Γ expressed in photons per atom per second[13] is a function of temperature because a certain amount of light is lost to counteract relaxation in the maser. However, the medium becomes transparent, to some extent, upon optical pumping and the light penetrates into the central region of the cavity. In other words, the mean free path of the light inside the cell is increased by the light itself due to its unsymmetrical nature.[14] Γ is thus a parameter which is fixed for a given situation; it is best determined by a measurement on the maser itself.

(2) Relaxation. The master equation for relaxation is[15]

$$\frac{d\rho_{\mu\mu}}{dt}=\sum_{\mu'}\rho_{\mu'\mu'}W_{\mu'\mu}-\rho_{\mu\mu}W_{\mu\mu'}, \tag{10}$$

where $W_{\mu'\mu}$ is the rate of transition from level μ' to level μ. We assume that relaxation takes place uniformly among all the eight levels and we write

$$d\rho_{\mu\mu}/dt=-\gamma_1(\rho_{\mu\mu}-\tfrac{1}{8}). \tag{11a}$$

We also write

$$d\rho_{\mu\mu'}/dt=-\gamma_2\rho_{\mu\mu'}. \tag{11b}$$

We have defined $\gamma_1=8W_{\mu'\mu}$, the rate of decay to equilibrium of any diagonal elements. The decay of the off-diagonal elements is characterized by a rate γ_2. Both γ_1 and γ_2 contain contributions from buffer-gas collisions, spin-exchange collisions and collisions between rubidium atoms and the wall of the storage cell. Any other relaxation mechanism can be introduced in a similar phenomenological way. γ_1 and γ_2 are respectively $1/T_1$ and $1/T_2$.

(3) Radiation. The radiation term is calculated from the expression

$$\frac{d\rho_{\mu\mu'}}{dt}=\frac{i}{\hbar}\sum_k(\rho_{\mu k}H_{k\mu'}-H_{\mu k}\rho_{k\mu'}), \tag{12}$$

where $H_{k\mu'}$ and $H_{\mu k}$ are the matrix elements of the interaction with the rf field.

From these three mechanisms a set of eight equations is written for the diagonal elements of the density matrix. One equation is sufficient for the off-diagonal element, ρ_{73}. These equations are

$$d\rho_{\mu\mu}/dt=\tfrac{1}{8}\Gamma(\rho_{66}+\rho_{77}+\rho_{88})-\gamma_1(\rho_{\mu\mu}-\tfrac{1}{8}) \tag{13}$$

for $\mu=1, 2, 4, 5$;

$$d\rho_{33}/dt=\tfrac{1}{8}\Gamma(\rho_{66}+\rho_{77}+\rho_{88})-\gamma_1(\rho_{33}-\tfrac{1}{8})+2\beta\ \mathrm{Im}\rho_{73}e^{-i\omega t}, \tag{14}$$

$$d\rho_{\mu\mu}/dt=-\Gamma\rho_{\mu\mu}+\tfrac{1}{8}\Gamma(\rho_{66}+\rho_{77}+\rho_{88})-\gamma_1(\rho_{\mu\mu}-\tfrac{1}{8}) \tag{15}$$

for $\mu=6, 8$;

$$d\rho_{77}/dt=-\Gamma\rho_{77}+\tfrac{1}{8}\Gamma(\rho_{66}+\rho_{77}+\rho_{88})-\gamma_1(\rho_{77}-\tfrac{1}{8})-2\beta\ \mathrm{Im}\rho_{73}e^{-i\omega t}, \tag{16}$$

$$d\rho_{73}/dt=i\omega_0\rho_{73}-i\beta(\rho_{33}-\rho_{77})\times e^{i\omega t}-(\tfrac{1}{2}\Gamma+\gamma_2)\rho_{37}-i\Delta\omega_l\rho_{73}, \tag{17}$$

where $\beta=\frac{1}{2}(\mu_0H_z/\hbar)$, ω_0 is the atomic resonant frequency, and ω is the frequency of the applied field H_z.

b. Maser equation. The solution of this set of equations is done at equilibrium as in the case of the hydrogen maser.[16–18] The power delivered by the rubidium vapor is given by $Nh\nu(d\rho_{33}/dt)_{\mathrm{rad}}$ and is calculated as

$$P=Nh\nu\times\frac{2\langle\beta^2\rangle\Gamma A}{(\frac{1}{2}\Gamma+\gamma_2)+[\gamma_1/(\frac{1}{2}\Gamma+\gamma_2)](\omega-\omega')^2+(1+\Gamma B)4\langle\beta^2\rangle}, \tag{18}$$

where

$$A=\gamma_1(\Gamma+\gamma_1)/(5\Gamma^2+13\gamma_1\Gamma+8\gamma_1^2), \tag{19}$$

$$B=(3\Gamma+4\gamma_1)/(5\Gamma^2+13\gamma_1\Gamma+8\gamma_1^2), \tag{20}$$

$$\omega'=\omega_0-\Delta\omega_l. \tag{21}$$

In the presence of a buffer gas the atoms are assumed to be at rest and β^2 has been averaged over the cavity volume.[19] The field created by the rubidium atoms is made self-consistent by equating the radiated power to the dissipated power. The relation between the rf field and the power dissipated in the cavity is

$$4\langle\beta^2\rangle=(8\pi Q_l\eta\mu_0{}^2/\omega V_c\hbar^2)P_{\mathrm{diss}};$$

from this relation and Eq. (18) we arrive at the maser equation[20]

$$\frac{P}{P_m}=\left[\frac{\Gamma'}{\Gamma_m'}\frac{\Gamma'+1}{(2\Gamma'^2+9\Gamma'+8)}-\frac{(\frac{1}{2}\Gamma'+r)(5\Gamma'^2+13\Gamma'+8)}{(2\Gamma'^2+9\Gamma'+8)}\right], \tag{22}$$

where

$$\Gamma_m'=\gamma_1\hbar/4n\pi Q_l\eta\mu_0{}^2=\Gamma_m/\gamma_1, \tag{23}$$

$$\Gamma'=\Gamma/\gamma_1, \tag{24}$$

$$P_m=\tfrac{1}{2}Nh\nu\Gamma_m, \tag{25}$$

$$r=\gamma_2/\gamma_1. \tag{26}$$

---

[13] C. O. Alley, Palmer Physical Lab, Princeton University Report, 1960 (unpublished).

[14] The detailed solution for the case where the pumping rate and the density matrix elements are a function of position in the maser cell is being carried out on a computer in collaboration with W. Happer of Columbia University.

[15] C. P. Slichter, *Principles of Magnetic Resonance* (Harper and Row, New York, 1963).

[16] D. Kleppner, H. C. Berg, S. B. Crampton, N. F. Ramsey, R. F. C. Vessot, H. E. Peters, and J. Vanier, Phys. Rev. **138**, A972 (1965).

[17] P. L. Bender, Phys. Rev. **136**, 2154 (1964).

[18] J. Vanier and R. F. C. Vessot, IEEE J. Quantum Electron. **9**, 391 (1966).

[19] D. Kleppner, H. M. Goldenberg, and N. F. Ramsey, Phys. Rev. **126**, 603 (1962).

[20] A similar expression can be derived for the Rb^{85} maser. It is

$$\frac{P}{P_m}=\left[\frac{\Gamma'}{\Gamma_m'}\frac{\Gamma'+1}{(3\Gamma'^2+13\Gamma'+12)}-\frac{(\frac{1}{2}\Gamma'+r)(7\Gamma'+19\Gamma'+12)}{(3\Gamma'^2+13\Gamma'+12)}\right].$$

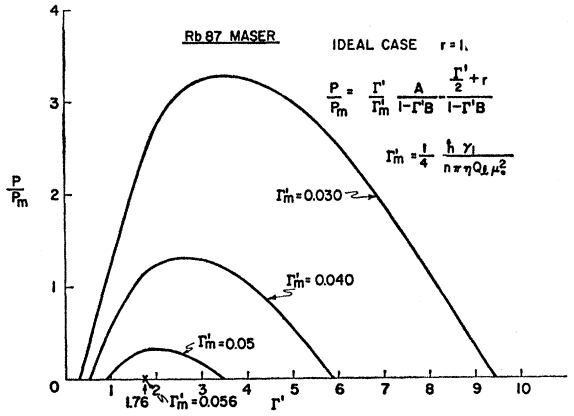

FIG. 3. Variation of power output versus rubidium maser versus light intensity for several values of the oscillation parameter Γ_m'.

The various parameters are defined as follows: n is the rubidium density; N is the total number of atoms; Q_l is cavity quality factor; η is the filling factor; μ_0 is the Bohr magneton; ν is the resonance frequency. Figure 3 shows the variation of P/P_m with the normalized pumping rate Γ' for several values of Γ_m'.

(1) Oscillation parameter. Γ_m' is called the oscillation parameter in a similar sense as q in the hydrogen maser.[16] By requiring the power output to be positive (oscillating state) we can set a limit on Γ_m'. That limit is

$$\Gamma_m' \leq [(\sqrt{80r})+4+5r]^{-1}. \tag{27}$$

In order to determine if oscillations are possible, one needs to know the ratio of γ_2 to γ_1. Experiments have shown that in a buffer gas such as nitrogen, dephasing collisions are more frequent than collisions which affect the populations of the states. Thus at low rubidium pressures where the spin-exchange dephasing action between rubidium atoms is small relative to interactions with the buffer gas, we expect r to be large.[10] At temperatures of the order of 65°C where spin-exchange interactions contribute to a large extent to the relaxation, we find experimentally that r is close to 1. Consequently, the minimum value of Γ_m' necessary for oscillation varies with the density of rubidium. In the case $r=1$, Γ_m' needs to be smaller than 0.056.

(2) Filling factor. Because of the presence of the buffer gas, rubidium atoms are confined to an rf field of the same phase during the time of emission. In the case where the bulb completely fills the cavity, one calculates for a TE_{0n1} cylindrical cavity

$$\eta = \langle H_z^2 \rangle_{\text{bulb}} / \langle H^2 \rangle_{\text{cavity}} = \lambda_0^2/\lambda_c^2, \tag{28}$$

where λ_0 is the free-space wavelength of the microwave radiation and λ_c is the cut-off wavelength of a cylindrical waveguide of the same diameter as the cavity.

2. *Transient Operation*

In the previous section the theory of the rubidum maser has been derived and a closed-form solution has been obtained. This theory was developed on the assumption that a steady-state situation exists in the maser. By this it is meant that parameters such as light intensity and rf amplitude are kept constant with time. There are experiments, however, in which more information is obtained by operating the maser under transient operation. For example, the light may be applied in the form of pulses followed by rf pulses which send the atomic system into a radiant state. Experiments of this nature have been reported by Arditi *et. al.*[21] The present experimental arrangement with its high maser gain, however, permits experiments which could not be performed in their case.

This mode of operation is probably the one that gives most information. The rf pulse produces a ringing in the maser and the decay of this induced signal is a function of the relaxation time and oscillation parameter. It has been found possible to determine the rubidium spin-exchange cross section through this technique. In the present section the theory of such a transient operation is described. The starting point of the analysis is found in Eqs. (14), (16), and (17) of the previous section. We define

$$\Delta = \rho_{33} - \rho_{77}, \tag{29}$$

$$\rho_{73} = \delta e^{i\omega t}, \tag{30}$$

where δ is time-dependent. To arrive at Eq. (18), ρ_{73} was assumed to have the form given here with the difference, however, that an equilibrium was assumed in which δ was a constant.

Assuming resonance, we can write $\omega=\omega_0$ and we obtain the two following simple equations in the dark where $\Gamma=0$:

$$d\Delta/dt = 4\beta\ \text{Im}\delta - \gamma_1\Delta, \tag{31}$$

$$d\delta/dt = -i\beta\Delta - \gamma_2\delta, \tag{32}$$

where β is a measure of the rf field in the cavity. The above set of equations has been solved for a typical experimental situation represented in Fig. 4. The light pulse is first applied and creates a difference in population between levels 3 and 7. Immediately after the pulse, this difference is Δ_0. A resonant microwave pulse is applied at some time t later and induces the atomic system into a radiant state in which it emits energy in the form of microwaves.

The amplitude of the induced signal is proportional to the residual difference of population at the time t after the light pulse. By varying the time t, the initial amplitude of the induced signal traces the decay of the population difference between the two levels contributing to the signal. On the other hand the decay of the induced signal is caused by buffer gas and spin-exchange collisions; as will be shown later, the decay may also, in certain experimental situations, reflect the effect of the rf field on the atoms themselves.

[21] M. Arditi and T. R. Carver, Phys. Rev. 136, A643 (1964).

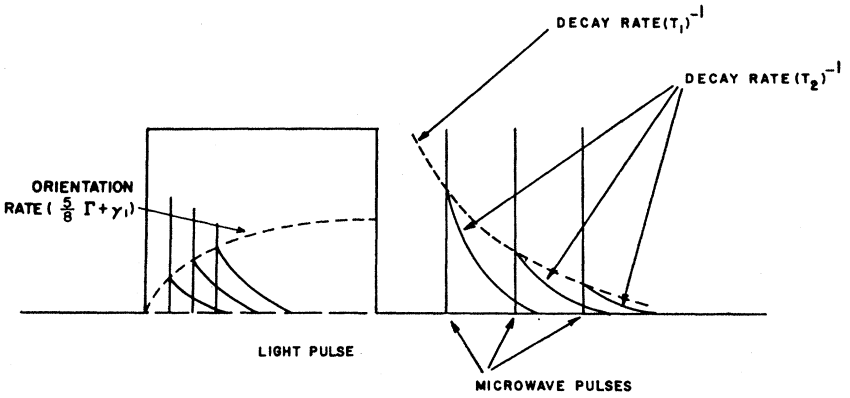

FIG. 4. Typical pulse sequence used in experiments described in this report. The growth of the orientation is traced by varying the time between the beginning of the light pulse and the microwave pulse. The decay rate of the orientation is traced by varying the time between the microwave pulse and the end of the light pulse. In each case the traces of the growth and decay may be obtained by multiple exposure on the oscillograph.

Another situation also shown in Fig. 4 is that where the microwave pulse is applied during the light pulse at a given time after the light has been turned on. In that case the initial amplitude of the induced signal immediately after the microwave pulse measures the population difference obtained between the levels contributing to the signal. By varying the time t, the build-up of the rubidium-vapor orientation is traced, and the pumping rate can be obtained from this trace. The decay of the induced signal while the light is on, on the other hand, is controlled by decorrelation due to buffer-gas collisions, spin-exchange interaction, and the light itself. In the case where the system gain is high, enhancement may be observed in the decay. The enhancement may be large enough to produce a continuous oscillation during the light pulse. Examples of the various situations described above are presented in Fig. 5, in which are shown some multiple-exposure photographs of selected stimulated emission signals.

a. Solution during the microwave pulse (in the dark). In this case, β is constant and is called β_p. The solution of Eqs. (31) and (32) is then[22]

$$\delta=(-i\Delta_0\beta_p/s)e^{-(1/2)(\gamma_1+\gamma_2)t}\sin st, \tag{33}$$

$$\Delta=\Delta_0 e^{-(1/2)(\gamma_1+\gamma_2)t}\left[\cos st+\frac{(\gamma_2-\gamma_1)}{2s}\sin st\right], \tag{34}$$

where

$$s=[4\beta_p{}^2-\tfrac{1}{4}(\gamma_2-\gamma_1)^2]^{1/2} \tag{35}$$

and t is measured from the beginning of the microwave pulse.

In a typical experimental situation, the pulse length is so short that there is practically no relaxation taking place and $e^{-\gamma t}\approx 1$. In that case, calling the pulse length τ, we can write $2\beta_p\tau=\theta_p$ and we obtain

$$\delta=-\tfrac{1}{2}i\Delta_0\sin\theta_p, \tag{36}$$

$$\Delta=\Delta_0\cos\theta_p. \tag{37}$$

A 90° pulse is one that makes Δ equal to zero and δ maximum.

b. Solution after the microwave pulse (in the dark). The solution of Eqs. (31) and (32), after the microwave pulse, is complicated by the fact that β is not constant. Two cases are considered. First, one assumes that after the pulse the microwave field is so small that it does not influence the populations. In other words, the radiation lifetime is much longer than the relaxation time. In that case, measuring time t_1 from the end of the light pulse,

$$\Delta(t_1)=\Delta_0 e^{-\gamma_1 t_1}, \tag{38}$$

$$\delta=\delta(\theta_p)e^{-\gamma_2(t-t_1)}, \tag{39}$$

where $\delta(\theta_p)$ is the value of δ after a microwave pulse of phase angle θ_p and $\Delta(t_1)$ is the value of Δ at time t_1 after the light pulse. The power radiated by the atoms after the pulse is given by

$$P=-\tfrac{1}{2}h\nu N(d\Delta/dt)_{\text{rad}} \tag{40}$$

and the field is then given by the equation

$$4\langle\beta^2\rangle=-k(d\Delta/dt)_{\text{rad}}, \tag{41}$$

where

$$k=(8\pi Q_l\eta\mu_0{}^2/2V_c\hbar)N. \tag{42}$$

The radiation term $(d\Delta/dt)_{\text{rad}}$ is obtained from Eq. (31) and

$$\beta=-k\delta=-k\delta(\theta_p)e^{-\gamma_2(t-t_1)}, \tag{43}$$

$$P=2\hbar\omega Nk[\delta(\theta_p)]^2e^{-2\gamma_2(t-t_1)}. \tag{44}$$

Thus the field in the cavity decays at the rate γ_2 and the power at the rate $2\gamma_2$. With a linear detector the rate γ_2 is measured directly.

The amplitude $\delta(\theta_p)$, on the other hand, is proportional to the value of Δ at time t_1. Consequently a plot of the field amplitude immediately after the microwave pulse versus t_1 gives information on Δ and on the rate γ_1. This is illustrated in Figs. 4 and 5(a).

The second case of importance is the one where the effect of the radiation field is comparable to the effect of the relaxation. In that case, Eqs. (31), (32), and (41) have to be solved simultaneously. This set of equations can be solved exactly for the case $\gamma_1=\gamma_2$. The solution is

$$\delta=-i\tfrac{1}{2}\Delta_0 e^{-\gamma t}\operatorname{sech}[-(\Delta_0 k/\gamma)\times(1-e^{-\gamma t})-\ln\tan\tfrac{1}{2}\theta_p], \tag{45}$$

[22] H. C. Torrey, Phys. Rev. 76, 1059 (1949).

$$\Delta=\Delta_0 e^{-\gamma t}\tanh[-(\Delta_0 k/\gamma)(1-e^{-\gamma t})-\ln\tan\tfrac{1}{2}\theta_p], \quad (46)$$

$$P=\tfrac{1}{2}h\nu N k_0\Delta_0^2 e^{-2\gamma t}\operatorname{sech}^2[-(\Delta_0 k/\gamma)\times(1-e^{-\gamma t})-\ln\tan\tfrac{1}{2}\theta_p]. \quad (47)$$

The above equations are the same as those obtained by Bloom[23] in a different mathematical context. Equation (47) predicts a delayed surge of power with a maximum at a time t_M after the microwave pulse. This time is obtained by differentiating P in respect to t for a given microwave pulse phase angle and is given by the equation

$$1=(\Delta_0 k/\gamma)e^{-\gamma t_M}\tanh[-(\Delta_0 k/\gamma)\times(1-e^{-\gamma t_M})-\ln\tan\tfrac{1}{2}\theta_p]. \quad (48)$$

When t_M tends to zero the above relation becomes

$$\Delta_0 k/\gamma=(\cos\theta_p)^{-1}|_{t_M=0}=a. \quad (49)$$

The value of θ_p for this situation can be determined experimentally. From the definition of k and the relation $\gamma_1\simeq n\bar{v}_r\sigma$, where $\bar{v}_r$ is the relative velocity, n is the density, and σ the spin-exchange cross section, one can write

$$\sigma=(4\pi\mu_0^2/\hbar\bar{v}_r)(\Delta_0 Q_l\eta V_b/V_c)(\cos\theta_p)|_{t_M=0}. \quad (50)$$

The above equation provides a means of determining the spin-exchange cross section without a previous knowledge of the density.

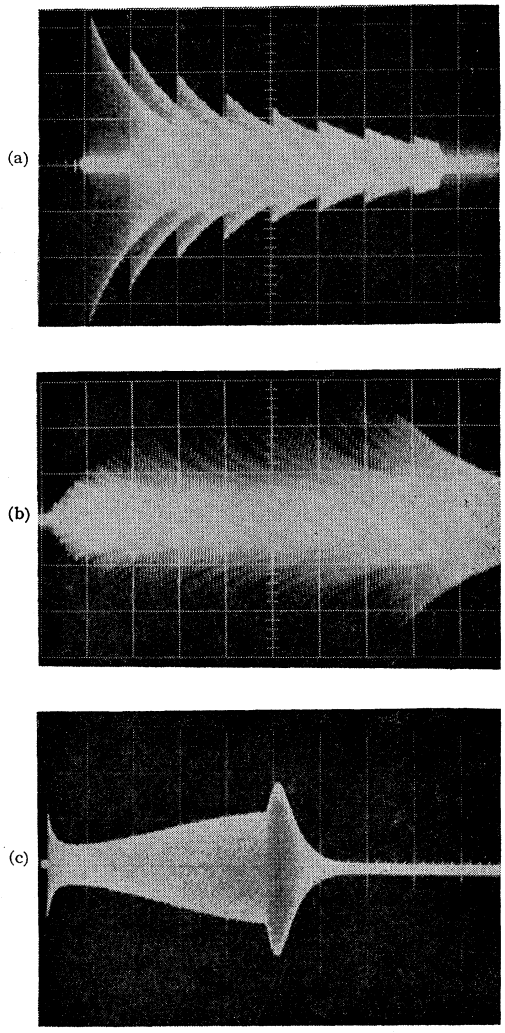

FIG. 5. Typical experimental results. Photograph (a) shows a multiple exposure of the induced signal after the microwave pulse. The time base is 10 msec/div and the trace is triggered by the end of the light pulse. Photograph (b) is a multiple exposure of the growth of the orientation during the light pulse; in that case the trace is triggered from the beginning of the light pulse. The time base is 1 msec/div. In photograph (c), the maser gain is sufficiently high to permit continuous oscillation. The time base is 10 msec/div and the scope is triggered from the beginning of the light pulse. The light pulse ends at about 48 msec where the power output rises because the decorrelation effect of the light is removed.

c. Pumping rate Γ. At the beginning of the light pulse, the distribution of atoms among the levels varies with time; if the pulse of light is sufficiently long, equilibrium among the levels is reached. Equations (14), (15), and (16) can be solved in the transient state in the case $\beta=0$ .The result is

$$\Delta=\left[\frac{\Gamma}{5\Gamma+8\gamma_1}\right][1-e^{-[(5/8)\Gamma+\gamma_1]t}], \quad (51)$$

where time is measured from the beginning of the light pulse. The characteristic time for redistribution of the atoms among the energy levels by the light is thus $(\frac{5}{8}\Gamma+\gamma_1)^{-1}$.

In practice the population difference Δ is monitored with a probing rf pulse and the characteristic time $(\frac{5}{8}\Gamma+\gamma_1)^{-1}$ is measured as shown in Fig. 4. From a measurement of γ_1, through the method described earlier, we finally arrive at the determination of Γ. Figure 5(b) shows a multiple-exposure photograph tracing the growth of Δ.

B. Spin Exchange in Rb^{87}

Detailed calculations of spin-exchange interactions have been made for hydrogen by Wittke,[24] who considered the case of strong collisions in which the relative phase between the singlet and triplet wave function of the two-atom system is randomized by the collision. More recently, Bender[17] has made calculations for hydrogen spin-exchange interactions not limited to the case of strong collisions. A feature of the calculations is the prediction of a small frequency shift of the atomic resonance of about 5% of the spin-exchange linewidth.

We have applied the theory developed by Bender to the case of rubidium spin-exchange collisions. His Eq. (6) is repeated here with a slight change in notation:

$$\sigma^f=\sigma^i-(1-\cos\Delta\varphi)(c\sigma^i+\sigma^i c-2c\sigma^i c)-i4\sin\Delta\varphi(\sigma^i c-c\sigma^i), \quad (52)$$

[23] S. Bloom, J. Appl. Phys. **27**, 785 (1956).

[24] J. P. Wittke, thesis, Princeton University, 1955 (unpublished).

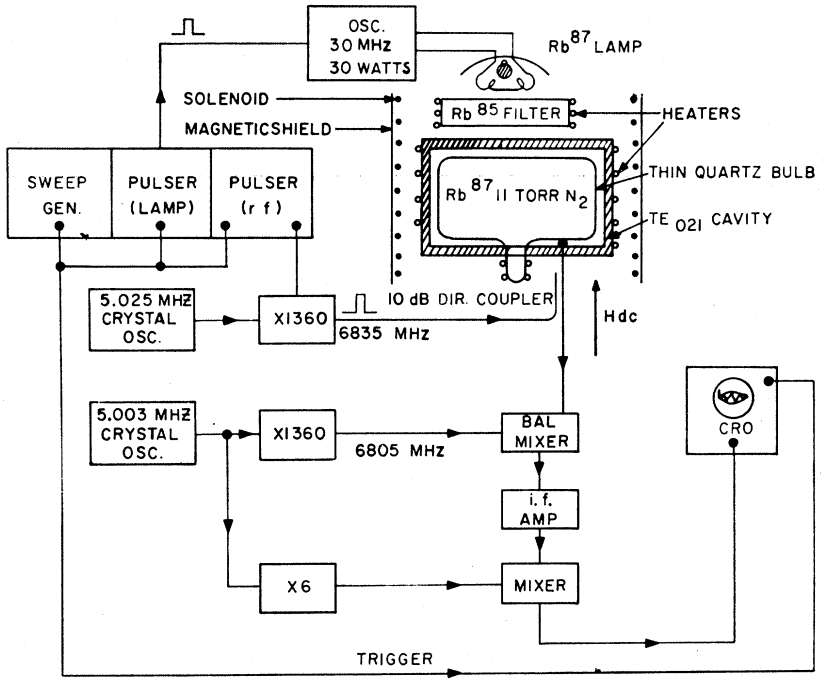

FIG. 6. Block diagram of the measuring apparatus.

where σ^f and σ^i are respectively the final and initial density matrices of the two-atom system. The matrix C is defined as $C=M^+BM$, where M is the representation transformation matrix from the S representation, in which the two electron spins and the two nuclear spins are coupled, to the F representation where the electron and nuclear spins are coupled.[25] B is a matrix, related to the spin-exchange matrix operator; it is diagonal with all elements zero except for the last eight which are equal to 1. $\Delta\varphi$ is the phase shift between the triplet and singlet part of the wave function due to the collision.

Matrices M and C are all of order 64. They have been calculated in detail. Matrix C is given in Table I in the form of 16 matrices of order 16 in the following notation:

$$C=\begin{Bmatrix}11 & 12 & 13 & 14\\ 21 & 22 & 23 & 24\\ 31 & 32 & 33 & 34\\ 41 & 42 & 43 & 44\end{Bmatrix}.$$

In Table I the 16×16 matrices are called C_{11}, C_{12}, etc. All the elements not written are zero; those elements which are zero and which are written in the C matrix, originate from the property of the Wigner coefficients and are kept here to preserve the symmetry of the matrix.

It can be shown from the properties of the matrices M and B that

$$c_{ij}=\sum_k c_{ik}c_{kj}. \tag{53}$$

This property can be used to check the final results.

[25] M is used here instead of Γ, to avoid confusion with the pumping rate defined earlier in this article.

Defining the spin-exchange cross section as

$$\sigma=\frac{1}{2}\left[2\pi\int(1-\cos\Delta\varphi(R))RdR\right], \tag{54}$$

where R is the impact parameter, one finally obtains that the rate of change of $(\rho_{33}-\rho_{77})$; and $\rho_{37}=\delta e^{i\omega t}$, due to spin-exchange collisions, is given by

$$d(\rho_{33}-\rho_{77})/dt=-n\bar{v}_r\sigma(\rho_{33}-\rho_{77}), \tag{55}$$

$$d\rho_{37}/dt=-n\bar{v}_r\sigma\rho_{37}(\tfrac{5}{8}-\tfrac{1}{8}[-\rho_{11}+\tfrac{1}{2}\rho_{22}+\rho_{33}+\tfrac{1}{2}\rho_{44}-\rho_{55}-\tfrac{1}{2}\rho_{66}+\rho_{77}-\tfrac{1}{2}\rho_{88}])-i\sin\Delta\varphi(\rho_{33}-\rho_{77}). \tag{56}$$

The last term of Eq. (56) introduces a small frequency shift in the atomic resonance. The part in the square bracket in the first term of the same equation is very small in most experimental situations and can be neglected. From Eq. (56) it is seen that the ratio γ_1/γ_2 for spin exchange is approximately 8/5. Experimental results reported later in this paper confirm this prediction. This is to be compared to the case of hydrogen where this ratio is 2.[24]

III. APPARATUS

The measurements reported below have been made with the experimental arrangement shown in Fig. 6. The pulsers and receiver were commercially available items. The multiplier chains were specially built for the frequency of interest here. The rubidium lamp consisted of a 1-in. bulb filled with a few milligrams of Rb^{87} and 2 Torr of krypton, placed in the tank circuit of an rf oscillator. The power delivered to the bulb was of the order of 30 W. In one case the bulb was placed inside

TABLE I. Matrix C for electron spin exchange in rubidium-87. The matrix shown here is $\frac{1}{4}$ of the matrix that would be obtained in Bender's notation.

C_{11}

F_1M_1 \ F_2M_2	22	21	20	2–1	2–2	1–1	10	11	22	21	20	2–1	2–2	1–1	10	11
22	0															
21		$\frac{1}{8}$						$\frac{1}{8}\sqrt{3}$	$-\frac{1}{8}$							
20			0				$\frac{1}{4}$			$-\frac{1}{8}\sqrt{\frac{3}{2}}$						$\frac{1}{4}\sqrt{\frac{1}{8}}$
2–1				$\frac{3}{8}$		$\frac{1}{8}\sqrt{3}$					$-\frac{1}{8}\sqrt{\frac{3}{2}}$			$\frac{1}{8}\sqrt{\frac{3}{2}}$		
2–2					$\frac{1}{2}$							$-\frac{1}{8}$		$\frac{1}{8}\sqrt{3}$		
1–1				$\frac{1}{8}\sqrt{3}$		$\frac{1}{8}$					$-\frac{1}{8}\sqrt{\frac{1}{2}}$				$\frac{1}{8}\sqrt{\frac{1}{2}}$	
10			$\frac{1}{4}$				$\frac{1}{4}$			$-\frac{1}{8}\sqrt{\frac{3}{2}}$						$\frac{1}{4}\sqrt{\frac{1}{8}}$
11		$\frac{1}{8}\sqrt{3}$						$\frac{3}{8}$	$-\frac{1}{8}\sqrt{3}$							
22		$-\frac{1}{8}$						$-\frac{1}{8}\sqrt{3}$	$\frac{1}{8}$							
21			$-\frac{1}{8}\sqrt{\frac{3}{2}}$				$-\frac{1}{8}\sqrt{\frac{3}{2}}$			$\frac{3}{16}$						$\frac{1}{16}\sqrt{3}$
21				$-\frac{1}{8}\sqrt{\frac{3}{2}}$		$-\frac{1}{8}\sqrt{\frac{1}{2}}$					$\frac{1}{4}$				$\frac{1}{8}$	
21					$-\frac{1}{8}$							$\frac{5}{16}$		$\frac{1}{16}\sqrt{3}$		
21													$\frac{3}{8}$			
21					$\frac{1}{8}\sqrt{3}$							$\frac{1}{16}\sqrt{3}$		$\frac{1}{8}$		
21				$\frac{1}{8}\sqrt{\frac{3}{2}}$		$\frac{1}{8}\sqrt{\frac{1}{2}}$					$\frac{1}{8}$				$\frac{1}{4}$	
21			$\frac{1}{4}\sqrt{\frac{1}{8}}$				$\frac{1}{4}\sqrt{\frac{1}{8}}$			$\frac{1}{16}\sqrt{3}$						$\frac{5}{16}$

C_{21}

F_1M_1 \ F_2M_2	22	21	20	2–1	2–2	1–1	10	11	22	21	20	2–1	2–2	1–1	10	11
20			0				0			$-\frac{1}{8}\sqrt{\frac{3}{2}}$						$-\frac{3}{4}\sqrt{\frac{1}{8}}$
20				0		0					$-\frac{3}{16}$				$-\frac{3}{16}$	
20					0							$-\frac{3}{16}$		$-\frac{1}{16}\sqrt{3}$		
20													$-\frac{1}{8}\sqrt{\frac{3}{2}}$			
20																
20													$\frac{3}{8}\sqrt{\frac{1}{2}}$			
20					0							$\frac{3}{16}$		$\frac{1}{16}\sqrt{3}$		
20				0		0					$\frac{1}{16}\sqrt{3}$				$\frac{1}{16}\sqrt{3}$	
2–1				0		0					0				0	
2–1					0							0		0		
2–1													0			
2–1																
2–1																
2–1																
2–1													0			
2–1					0							0		0		

C_{31}

F_1M_1 \ F_2M_2	22	21	20	2–1	2–2	1–1	10	11	22	21	20	2–1	2–2	1–1	10	11
2–2					0							0		0		
2–2													0			
2–2																
2–2																
2–2																
2–2																
2–2																
2–2													0			
1–1				0		0					0				0	
1–1					0							0		0		
1–1													0			
1–1																
1–1																
1–1																
1–1													0			
1–1					0							0		0		

TABLE I. (*continued*).

C_{41}

F_1M_1 \ F_2M_2	22	21	20	2–1	2–2	1–1	10	11	22	21	20	2–1	2–2	1–1	10	11
	22	22	22	22	22	22	22	22	21	21	21	21	21	21	21	21
10	22		0				0			$-\frac{1}{8}\sqrt{\frac{3}{2}}$						$-\frac{3}{4}\sqrt{\frac{1}{8}}$
10	21			0		0					$-\frac{3}{16}$				$-\frac{3}{16}$	
10	20				0							$-\frac{3}{16}$		$-\frac{1}{16}\sqrt{3}$		
10	2–1												$-\frac{1}{8}\sqrt{\frac{3}{2}}$			
10	2–2															
10	1–1												$\frac{3}{8}\sqrt{\frac{1}{2}}$			
10	10				0							$\frac{3}{16}$		$\frac{1}{16}\sqrt{3}$		
10	11			0		0					$\frac{1}{16}\sqrt{3}$				$\frac{1}{16}\sqrt{3}$	
11	22	$-\frac{1}{8}\sqrt{3}$						$-\frac{3}{8}$	$\frac{1}{8}\sqrt{3}$							
11	21		$-\frac{3}{4}\sqrt{\frac{1}{8}}$				$-\frac{3}{4}\sqrt{\frac{1}{8}}$			$\frac{1}{16}\sqrt{3}$						$-\frac{3}{16}$
11	20			$-\frac{3}{16}\sqrt{2}$		$-\frac{1}{8}\sqrt{\frac{3}{2}}$					0				$-\frac{1}{8}\sqrt{3}$	
11	2–1				$-\frac{1}{8}\sqrt{3}$							$-\frac{1}{16}\sqrt{3}$		$-\frac{3}{16}$		
11	2–2												$-\frac{1}{8}\sqrt{3}$			
11	1–1				$\frac{3}{8}$							$-\frac{3}{16}$		$\frac{1}{16}\sqrt{3}$		
11	10			$\frac{3}{16}\sqrt{2}$		$\frac{1}{8}\sqrt{\frac{3}{2}}$					$-\frac{1}{8}\sqrt{3}$				0	
11	11		$\frac{1}{8}\sqrt{\frac{3}{2}}$				$\frac{1}{8}\sqrt{\frac{3}{2}}$			$-\frac{3}{16}$						$-\frac{1}{16}\sqrt{3}$

C_{12}

F_1M_1 \ F_2M_2	22	21	20	2–1	2–2	1–1	10	11	22	21	20	2–1	2–2	1–1	10	11
	20	20	20	20	20	20	20	20	2–1	2–1	2–1	2–1	2–1	2–1	2–1	2–1
22	22															
22	21															
22	20	0														
22	2–1		0						0	0						
22	2–2			0				0			0					0
22	1–1		0						0	0						
22	10	0														
22	11															
21	22															
21	21	$-\frac{1}{8}\sqrt{\frac{3}{2}}$														
21	20		$-\frac{3}{16}$						$\frac{1}{16}\sqrt{3}$	0						
21	2–1			$-\frac{3}{16}$				$\frac{3}{16}$			0					0
21	2–2				$-\frac{1}{8}\sqrt{\frac{3}{2}}$		$\frac{3}{8}\sqrt{\frac{1}{2}}$					0			0	
21	1–1			$-\frac{1}{16}\sqrt{3}$				$\frac{1}{16}\sqrt{3}$			0					0
21	10		$-\frac{3}{16}$						$\frac{1}{16}\sqrt{3}$	0						
21	11	$-\frac{3}{4}\sqrt{\frac{1}{8}}$														

C_{22}

F_1M_1 \ F_2M_2	22	21	20	2–1	2–2	1–1	10	11	22	21	20	2–1	2–2	1–1	10	11
	20	20	20	20	20	20	20	20	2–1	2–1	2–1	2–1	2–1	2–1	2–1	2–1
20	22	$\frac{1}{4}$														
20	21		$\frac{1}{4}$					0	$-\frac{1}{8}\sqrt{\frac{3}{2}}$							
20	20			$\frac{1}{4}$			0			$-\frac{3}{16}$						$\frac{1}{16}\sqrt{3}$
20	2–1				$\frac{1}{4}$	0					$-\frac{3}{16}$				$\frac{3}{16}$	
20	2–2											$-\frac{1}{8}\sqrt{\frac{3}{2}}$		$\frac{3}{4}\sqrt{\frac{1}{8}}$		
20	1–1				0	$\frac{1}{4}$					$-\frac{1}{16}\sqrt{3}$				$\frac{1}{16}\sqrt{3}$	
20	10		0				$\frac{1}{4}$			$-\frac{3}{16}$						$\frac{1}{16}\sqrt{3}$
20	11	0						$\frac{1}{4}$	$-\frac{3}{8}\sqrt{\frac{1}{2}}$							
2–1	22	$-\frac{1}{8}\sqrt{\frac{3}{2}}$						$-\frac{3}{8}\sqrt{\frac{1}{2}}$	$\frac{3}{8}$							
2–1	21		$-\frac{3}{16}$				$-\frac{3}{16}$			$\frac{5}{16}$						$-\frac{1}{16}\sqrt{3}$
2–1	20			$-\frac{3}{16}$		$-\frac{1}{16}\sqrt{3}$					$\frac{1}{4}$				$-\frac{1}{8}$	
2–1	2–1				$-\frac{1}{8}\sqrt{\frac{3}{2}}$							$\frac{3}{16}$		$-\frac{1}{16}\sqrt{3}$		
2–1	2–2												$\frac{1}{8}$			
2–1	1–1				$\frac{3}{4}\sqrt{\frac{1}{8}}$							$-\frac{1}{16}\sqrt{3}$		$\frac{5}{16}$		
2–1	10			$\frac{3}{16}$		$\frac{1}{16}\sqrt{3}$					$-\frac{1}{8}$				$\frac{1}{4}$	
2–1	11		$\frac{1}{16}\sqrt{3}$				$\frac{1}{16}\sqrt{3}$			$-\frac{1}{16}\sqrt{3}$						$\frac{3}{16}$

TABLE I. (*continued*).

C_{32}

F_1M_1 \ F_2M_2	22	21	20	2–1	2–2	1–1	10	11	22	21	20	2–1	2–2	1–1	10	11
	20	20	20	20	20	20	20	20	2–1	2–1	2–1	2–1	2–1	2–1	2–1	2–1
2–2	22			0				0			$-\frac{1}{8}$					$-\frac{1}{8}\sqrt{3}$
2–2	21				0		0					$-\frac{1}{8}\sqrt{\frac{3}{2}}$				$-\frac{1}{8}\sqrt{\frac{3}{2}}$	
2–2	20					0							$-\frac{1}{8}\sqrt{\frac{3}{2}}$		$-\frac{1}{4}\sqrt{\frac{1}{8}}$		
2–2	2–1													$-\frac{1}{8}$			
2–2	2–2																
2–2	1–1													$\frac{1}{8}\sqrt{3}$			
2–2	10					0						$\frac{1}{8}\sqrt{\frac{3}{2}}$			$\frac{1}{4}\sqrt{\frac{1}{8}}$		
2–2	11				0		0				$\frac{1}{8}\sqrt{\frac{1}{2}}$					$\frac{1}{8}\sqrt{\frac{1}{2}}$	
1–1	22	$-\frac{1}{8}\sqrt{\frac{1}{2}}$							$-\frac{1}{8}\sqrt{\frac{3}{2}}$	$\frac{1}{8}\sqrt{3}$							
1–1	21		$-\frac{1}{16}\sqrt{3}$					$-\frac{1}{16}\sqrt{3}$		$\frac{1}{16}\sqrt{3}$							$-\frac{3}{16}$
1–1	20			$-\frac{1}{16}\sqrt{3}$		$-\frac{1}{16}$					0					$-\frac{1}{8}\sqrt{3}$	
1–1	2–1				$-\frac{1}{4}\sqrt{\frac{1}{8}}$							$-\frac{1}{16}\sqrt{3}$		$-\frac{3}{16}$			
1–1	2–2												$-\frac{1}{8}\sqrt{3}$				
1–1	1–1				$\frac{1}{8}\sqrt{\frac{3}{2}}$							$-\frac{3}{16}$		$\frac{1}{16}\sqrt{3}$			
1–1	10			$\frac{1}{16}\sqrt{3}$		$\frac{1}{16}$					$-\frac{1}{8}\sqrt{3}$				0		
1–1	11		$\frac{1}{16}$				$\frac{1}{16}$			$-\frac{3}{16}$							$-\frac{1}{16}\sqrt{3}$

C_{42}

F_1M_1 \ F_2M_2	22	21	20	2–1	2–2	1–1	10	11	22	21	20	2–1	2–2	1–1	10	11
	20	20	20	20	20	20	20	20	2–1	2–1	2–1	2–1	2–1	2–1	2–1	2–1
10	22	$\frac{1}{4}$															
10	21		$\frac{1}{8}$						$-\frac{1}{8}\sqrt{3}$	$\frac{1}{8}\sqrt{\frac{3}{2}}$							
10	20			0				$-\frac{1}{4}$			$\frac{3}{16}$						$-\frac{1}{16}\sqrt{3}$
10	2–1				$-\frac{1}{8}$		$-\frac{1}{8}\sqrt{3}$					$\frac{3}{16}$				$-\frac{3}{16}$	
10	2–2					$-\frac{1}{4}$							$\frac{1}{8}\sqrt{\frac{3}{2}}$		$-\frac{3}{4}\sqrt{\frac{1}{8}}$		
10	1–1				$-\frac{1}{8}\sqrt{3}$		$\frac{1}{8}$					$\frac{1}{16}\sqrt{3}$				$-\frac{1}{16}\sqrt{3}$	
10	10			$-\frac{1}{4}$				0			$\frac{3}{16}$						$-\frac{1}{16}\sqrt{3}$
10	11		$-\frac{1}{8}\sqrt{3}$						$-\frac{1}{8}$	$\frac{3}{8}\sqrt{\frac{1}{2}}$							
11	22																
11	21	$\frac{1}{4}\sqrt{\frac{1}{8}}$															
11	20		$\frac{1}{16}\sqrt{3}$						$-\frac{1}{16}$	0							
11	2–1			$\frac{1}{16}\sqrt{3}$				$-\frac{1}{16}\sqrt{3}$			0						0
11	2–2				$\frac{1}{8}\sqrt{\frac{1}{2}}$		$-\frac{1}{8}\sqrt{\frac{3}{2}}$					0				0	
11	1–1			$\frac{1}{16}$				$-\frac{1}{16}$			0						0
11	10		$\frac{1}{16}\sqrt{3}$						$-\frac{1}{16}$	0							
11	11	$\frac{1}{8}\sqrt{\frac{3}{2}}$															

C_{13}

F_1M_1 \ F_2M_2	22	21	20	2–1	2–2	1–1	10	11	22	21	20	2–1	2–2	1–1	10	11
	2–2	2–2	2–2	2–2	2–2	2–2	2–2	2–2	1–1	1–1	1–1	1–1	1–1	1–1	1–1	1–1
22	22																
22	21																
22	20																
22	2–1								0								
22	2–2	0								0							0
22	1–1								0								
22	10																
22	11																
21	22																
21	21																
21	20								0								
21	2–1	0								0					0		0
21	2–2		0					0			0					0	
21	1–1	0								0							0
21	10								0								
21	11																

TABLE I. (*continued*).

C_{23}

F_1M_1 \ F_2M_2	22	21	20	2–1	2–2	1–1	10	11	22	21	20	2–1	2–2	1–1	10	11
	2–2	2–2	2–2	2–2	2–2	2–2	2–2	2–2	1–1	1–1	1–1	1–1	1–1	1–1	1–1	1–1
20 22																
20 21									$-\frac{1}{8}\sqrt{\frac{1}{2}}$							
20 20	0									$-\frac{1}{16}\sqrt{3}$						$\frac{1}{16}$
20 2–1		0						0			$-\frac{1}{16}\sqrt{3}$				$\frac{1}{16}\sqrt{3}$	
20 2–2			0				0					$-\frac{1}{4}\sqrt{\frac{1}{8}}$		$\frac{1}{8}\sqrt{\frac{3}{2}}$		
20 1–1		0						0			$-\frac{1}{16}$				$\frac{1}{16}$	
20 10	0									$-\frac{1}{16}\sqrt{3}$						$\frac{1}{16}$
20 11									$-\frac{1}{8}\sqrt{\frac{3}{2}}$							
2–1 22									$\frac{1}{8}\sqrt{3}$							
2–1 21	$-\frac{1}{8}$									$\frac{1}{16}\sqrt{3}$						$-\frac{3}{16}$
2–1 20		$-\frac{1}{8}\sqrt{\frac{3}{2}}$						$\frac{1}{8}\sqrt{\frac{1}{2}}$			0				$-\frac{1}{8}\sqrt{3}$	
2–1 2–1			$-\frac{1}{8}\sqrt{\frac{3}{2}}$				$\frac{1}{8}\sqrt{\frac{3}{2}}$					$-\frac{1}{16}\sqrt{3}$		$-\frac{3}{16}$		
2–1 2–2				$-\frac{1}{8}$		$\frac{1}{8}\sqrt{3}$							$-\frac{1}{8}\sqrt{3}$			
2–1 1–1			$-\frac{1}{4}\sqrt{\frac{1}{8}}$				$\frac{1}{4}\sqrt{\frac{1}{8}}$					$-\frac{3}{16}$		$\frac{1}{16}\sqrt{3}$		
2–1 10		$-\frac{1}{8}\sqrt{\frac{3}{2}}$						$\frac{1}{8}\sqrt{\frac{1}{2}}$			$-\frac{1}{8}\sqrt{3}$				0	
2–1 11	$-\frac{1}{8}\sqrt{3}$									$-\frac{3}{16}$						$-\frac{1}{16}\sqrt{3}$

C_{33}

F_1M_1 \ F_2M_2	22	21	20	2–1	2–2	1–1	10	11	22	21	20	2–1	2–2	1–1	10	11
	2–2	2–2	2–2	2–2	2–2	2–2	2–2	2–2	1–1	1–1	1–1	1–1	1–1	1–1	1–1	1–1
2–2 22	$\frac{1}{2}$									$\frac{1}{8}\sqrt{3}$						$\frac{3}{8}$
2–2 21		$\frac{3}{8}$						$-\frac{1}{8}\sqrt{3}$			$\frac{3}{8}\sqrt{\frac{1}{2}}$				$\frac{3}{8}\sqrt{\frac{1}{2}}$	
2–2 20			$\frac{1}{4}$				$-\frac{1}{4}$					$\frac{3}{4}\sqrt{\frac{1}{8}}$		$\frac{1}{8}\sqrt{\frac{3}{2}}$		
2–2 2–1				$\frac{1}{8}$		$-\frac{1}{8}\sqrt{3}$							$\frac{1}{8}\sqrt{3}$			
2–2 2–2					0											
2–2 1–1				$-\frac{1}{8}\sqrt{3}$		$\frac{3}{8}$							$-\frac{3}{8}$			
2–2 10			$-\frac{1}{4}$				$\frac{1}{4}$					$-\frac{3}{4}\sqrt{\frac{1}{8}}$		$-\frac{1}{8}\sqrt{\frac{3}{2}}$		
2–2 11		$-\frac{1}{8}\sqrt{3}$						$\frac{1}{8}$			$-\frac{1}{8}\sqrt{\frac{3}{2}}$				$-\frac{1}{8}\sqrt{\frac{3}{2}}$	
1–1 22									$\frac{1}{8}$							
1–1 21	$\frac{1}{8}\sqrt{3}$									$\frac{3}{16}$						$\frac{1}{16}\sqrt{3}$
1–1 20		$\frac{3}{8}\sqrt{\frac{1}{2}}$						$-\frac{1}{8}\sqrt{\frac{3}{2}}$			$\frac{1}{4}$				$\frac{1}{8}$	
1–1 2–1			$\frac{3}{4}\sqrt{\frac{1}{8}}$				$-\frac{3}{4}\sqrt{\frac{1}{8}}$					$\frac{5}{16}$		$\frac{1}{16}\sqrt{3}$		
1–1 2–2				$\frac{1}{8}\sqrt{3}$		$-\frac{3}{8}$							$\frac{3}{8}$			
1–1 1–1			$\frac{1}{8}\sqrt{\frac{3}{2}}$				$-\frac{1}{8}\sqrt{\frac{3}{2}}$					$\frac{1}{16}\sqrt{3}$		$\frac{3}{16}$		
1–1 10		$\frac{3}{8}\sqrt{\frac{1}{2}}$						$-\frac{1}{8}\sqrt{\frac{3}{2}}$			$\frac{1}{8}$				$\frac{1}{4}$	
1–1 11	$\frac{3}{8}$									$\frac{1}{16}\sqrt{3}$						$\frac{5}{16}$

C_{43}

F_1M_1 \ F_2M_2	22	21	20	2–1	2–2	1–1	10	11	22	21	20	2–1	2–2	1–1	10	11
	2–2	2–2	2–2	2–2	2–2	2–2	2–2	2–2	1–1	1–1	1–1	1–1	1–1	1–1	1–1	1–1
10 22																
10 21									$\frac{1}{8}\sqrt{\frac{1}{2}}$							
10 20	0									$\frac{1}{16}\sqrt{3}$						$-\frac{1}{16}$
10 2–1		0						0			$\frac{1}{16}\sqrt{3}$				$-\frac{1}{16}\sqrt{3}$	
10 2–2			0				0					$\frac{1}{4}\sqrt{\frac{1}{8}}$		$-\frac{1}{8}\sqrt{\frac{3}{2}}$		
10 1–1		0						0			$\frac{1}{16}$				$-\frac{1}{16}$	
10 10	0									$\frac{1}{16}\sqrt{3}$						$-\frac{1}{16}$
10 11									$\frac{1}{8}\sqrt{\frac{3}{2}}$							
11 22																
11 21																
11 20									0							
11 2–1	0									0						0
11 2–2		0						0			0				0	
11 1–1	0									0						0
11 10									0							
11 11																

TABLE I. (*continued*).

C_{14}

F_1M_1 \ F_2M_2	22 10	21 10	20 10	2–1 10	2–2 10	1–1 10	10 10	11 10	22 11	21 11	20 11	2–1 11	2–2 11	1–1 11	10 11	11 11
22 22																
22 21									$-\frac{1}{8}\sqrt{3}$							
22 20	0									$-\frac{3}{4}\sqrt{\frac{1}{8}}$						$\frac{1}{8}\sqrt{\frac{3}{2}}$
22 2–1		0						0			$-\frac{3}{16}\sqrt{2}$				$\frac{3}{16}\sqrt{2}$	
22 2–2			0				0					$-\frac{1}{8}\sqrt{3}$		$\frac{3}{8}$		
22 1–1		0						0			$-\frac{1}{8}\sqrt{\frac{3}{2}}$				$\frac{1}{8}\sqrt{\frac{3}{2}}$	
22 10	0									$-\frac{3}{4}\sqrt{\frac{1}{8}}$						$\frac{1}{8}\sqrt{\frac{3}{2}}$
22 11									$-\frac{3}{8}$							
21 22									$\frac{1}{8}\sqrt{3}$							
21 21	$-\frac{1}{8}\sqrt{\frac{3}{2}}$									$\frac{1}{16}\sqrt{3}$						$-\frac{3}{16}$
21 20		$-\frac{3}{16}$						$\frac{1}{16}\sqrt{3}$			0				$-\frac{1}{8}\sqrt{3}$	
21 2–1			$-\frac{3}{16}$				$\frac{3}{16}$					$-\frac{1}{16}\sqrt{3}$		$-\frac{3}{16}$		
21 2–2				$-\frac{1}{8}\sqrt{\frac{3}{2}}$		$\frac{3}{8}\sqrt{\frac{1}{2}}$							$-\frac{1}{8}\sqrt{3}$			
21 1–1			$-\frac{1}{16}\sqrt{3}$				$\frac{1}{16}\sqrt{3}$					$-\frac{3}{16}$		$\frac{1}{16}\sqrt{3}$		
21 10		$-\frac{3}{16}$						$\frac{1}{16}\sqrt{3}$			$-\frac{1}{8}\sqrt{3}$				0	
21 11	$-\frac{3}{4}\sqrt{\frac{1}{8}}$									$-\frac{3}{16}$						$-\frac{1}{16}\sqrt{3}$

C_{24}

F_1M_1 \ F_2M_2	22 10	21 10	20 10	2–1 10	2–2 10	1–1 10	10 10	11 10	22 11	21 11	20 11	2–1 11	2–2 11	1–1 11	10 11	11 11
20 22	$\frac{1}{4}$									$\frac{1}{4}\sqrt{\frac{1}{8}}$						$\frac{1}{8}\sqrt{\frac{3}{2}}$
20 21		$\frac{1}{8}$							$-\frac{1}{8}\sqrt{3}$		$\frac{1}{16}\sqrt{3}$				$\frac{1}{16}\sqrt{3}$	
20 20			0					$-\frac{1}{4}$				$\frac{1}{16}\sqrt{3}$		$\frac{1}{16}$		
20 2–1				$-\frac{1}{8}$		$-\frac{1}{8}\sqrt{3}$							$\frac{1}{8}\sqrt{\frac{1}{2}}$			
20 2–2					$-\frac{1}{4}$											
20 1–1				$-\frac{1}{8}\sqrt{3}$		$\frac{1}{8}$							$-\frac{1}{8}\sqrt{\frac{3}{2}}$			
20 10			$-\frac{1}{4}$				0					$-\frac{1}{16}\sqrt{3}$		$-\frac{1}{16}$		
20 11		$-\frac{1}{8}\sqrt{3}$							$-\frac{1}{8}$		$-\frac{1}{16}$				$-\frac{1}{16}$	
2–1 22		$\frac{1}{8}\sqrt{\frac{3}{2}}$							$\frac{3}{8}\sqrt{\frac{1}{2}}$		0				0	
2–1 21			$\frac{3}{16}$					$\frac{3}{16}$				0		0		
2–1 20				$\frac{3}{16}$		$\frac{1}{16}\sqrt{3}$							0			
2–1 2–1					$\frac{1}{8}\sqrt{\frac{3}{2}}$											
2–1 2–2																
2–1 1–1					$-\frac{3}{4}\sqrt{\frac{1}{8}}$											
2–1 10				$-\frac{3}{16}$		$-\frac{1}{16}\sqrt{3}$							0			
2–1 11			$-\frac{1}{16}\sqrt{3}$				$-\frac{1}{16}\sqrt{3}$					0		0		

C_{34}

F_1M_1 \ F_2M_2	22 10	21 10	20 10	2–1 10	2–2 10	1–1 10	10 10	11 10	22 11	21 11	20 11	2–1 11	2–2 11	1–1 11	10 11	11 11
2–2 22			0				0					0		0		
2–2 21				0		0							0			
2–2 20					0											
2–2 2–1																
2–2 2–2																
2–2 1–1																
2–2 10					0											
2–2 11				0		0							0			
1–1 22		$\frac{1}{8}\sqrt{\frac{1}{2}}$							$\frac{1}{8}\sqrt{\frac{3}{2}}$			0			0	
1–1 21			$\frac{1}{16}\sqrt{3}$					$\frac{1}{16}\sqrt{3}$					0			
1–1 20				$\frac{1}{16}\sqrt{3}$		$\frac{1}{16}$								0		
1–1 2–1					$\frac{1}{4}\sqrt{\frac{1}{8}}$											
1–1 2–2																
1–1 1–1					$-\frac{1}{8}\sqrt{\frac{3}{2}}$											
1–1 10				$-\frac{1}{16}\sqrt{3}$		$-\frac{1}{16}$								0		
1–1 11			$-\frac{1}{16}$					$-\frac{1}{16}$					0		0	

TABLE I. (*continued*).

		C_{44}																
	F_2M_2	22	21	20	2–1	2–2	1–1	10	11	22	21	20	2–1	2–2	1–1	10	11
F_1M_1	F_1M_1 F_2M_2	10	10	10	10	10	10	10	10	11	11	11	11	11	11	11	11
10	22	$\frac{1}{4}$									$\frac{1}{4}\sqrt{\frac{1}{8}}$						$\frac{1}{8}\sqrt{\frac{3}{2}}$
10	21		$\frac{1}{4}$						0			$\frac{1}{16}\sqrt{3}$				$\frac{1}{16}\sqrt{3}$	
10	20			$\frac{1}{4}$				0					$\frac{1}{16}\sqrt{3}$		$\frac{1}{16}$		
10	2–1				$\frac{1}{4}$		0							$\frac{1}{8}\sqrt{\frac{1}{2}}$			
10	2–2					$\frac{1}{4}$											
10	1–1				0		$\frac{1}{4}$							$-\frac{1}{8}\sqrt{\frac{3}{2}}$			
10	10			0				$\frac{1}{4}$					$-\frac{1}{16}\sqrt{3}$		$-\frac{1}{16}$		
10	11		0						$\frac{1}{4}$			$-\frac{1}{16}$				$-\frac{1}{16}$	
11	22									$\frac{3}{8}$							
11	21	$\frac{1}{4}\sqrt{\frac{1}{8}}$									$\frac{5}{16}$						$-\frac{1}{16}\sqrt{3}$
11	20		$\frac{1}{16}\sqrt{3}$						$-\frac{1}{16}$			$\frac{1}{4}$				$-\frac{1}{8}$	
11	2–1			$\frac{1}{16}\sqrt{3}$				$-\frac{1}{16}\sqrt{3}$					$\frac{3}{16}$		$-\frac{1}{16}\sqrt{3}$		
11	2–2				$\frac{1}{8}\sqrt{\frac{1}{2}}$		$-\frac{1}{8}\sqrt{\frac{3}{2}}$							$\frac{1}{8}$			
11	1–1			$\frac{1}{16}$				$-\frac{1}{16}$					$-\frac{1}{16}\sqrt{3}$		$\frac{5}{16}$		
11	10		$\frac{1}{16}\sqrt{3}$						$-\frac{1}{16}$			$-\frac{1}{8}$				$\frac{1}{4}$	
11	11	$\frac{1}{8}\sqrt{\frac{3}{2}}$									$-\frac{1}{16}\sqrt{3}$						$\frac{3}{16}$

a light pipe made of polished copper tubing. Another lamp consisted similarly of a 1-in. bulb placed at the focus of a large spherical mirror. The power supply for these lamps was essentially that used by Alley.[13] The lamps could be pulsed at rates up to several kilohertz, and the decay time of the light pulse was of the order of a tenth of a millisecond. The lamps operated very satisfactorily and were sufficiently intense for the experiments to be reported. The only disadvantage was the amount of cooling required to maintain the optimum temperature. This was done by blowing air on the lamps. The maser was made of a copper cavity operated in a TE_{021} mode tuned to 6.835 GHz. The storage cells, filling the cavity almost entirely, were made of thin quartz to minimize microwave losses. Several designs of cells have been tried. Best results were obtained with a cell which had walls of the order of $\frac{3}{4}$ mm thick. The quality factor of the cavity-cell arrangement was 37 000. The transparent ends of the cavity were made of wrinkled copper foil. The maser could be illuminated with two lamps from either end.

IV. RESULTS

A. Buffer Gas Relaxation

To measure the contribution of the buffer gas to the relaxation, the maser cell was maintained at room temperature (about 26°C). At this temperature the rubidium density was low and relaxation by spin exchange was weak. The rubidium density was approximately 5×10^9 atoms per cc giving a spin-exchange contribution to γ_1 of approximately 4 sec^{-1}. This was small but still not negligible at the longest relaxation time measured. However, the results can be interpreted correctly if one allows for this added relaxation.

The relaxation times T_1 and T_2 were measured by the method described above. The experiments were performed with the cell open to a vacuum system. The best vacuum obtained with the oil-diffusion pump used was approximately 3×10^{-6}. The buffer gas was introduced into the bulb at the desired pressure through a play of stopcocks. The gases used were nitrogen and neon in glass bottles (Airco-assayed reagent). The pressure was measured with a Bourdon pressure gauge.

The results are shown in Fig. 7 for nitrogen as a buffer gas. The maximum of T_2 was observed at 8 Torr while the maximum of T_1 appeared between 15 and 20 Torr. The pressure at which the scattered radiation was quenched at maximum and where optical pumping was optimum was found by measuring the size of the signal immediately after the light pulse; this pressure was found to be 10 Torr with a broad maximum. From these results the pressure for maximum maser gain is between 10 and 15 Torr and does not appear to be too critical. This is in agreement with the results of Davidovits who measured the maser gain directly as a function of buffer gas pressure.[6]

The results obtained for neon were similar to those for nitrogen although the relaxation times at maximum were a little longer. The signals were weaker, probably because neon does not quench the scattered radiation that interacts with both hyperfine levels of the ground state, destroying to a certain extent the orientation obtained. A maximum of 70 msec was observed for T_1 at a pressure of 30 Torr. T_2 had a maximum of 13.5 msec at a pressure of 20 Torr.

It is observed that the maximum value of T_1 observed in these experiments is around 70 msec. In a bulb that had been sealed for several months, T_1 was as long as 85 msec at room temperature. Applying a correction for the presence of rubidium spin-exchange interaction at the temperature of operation, the relaxation time due

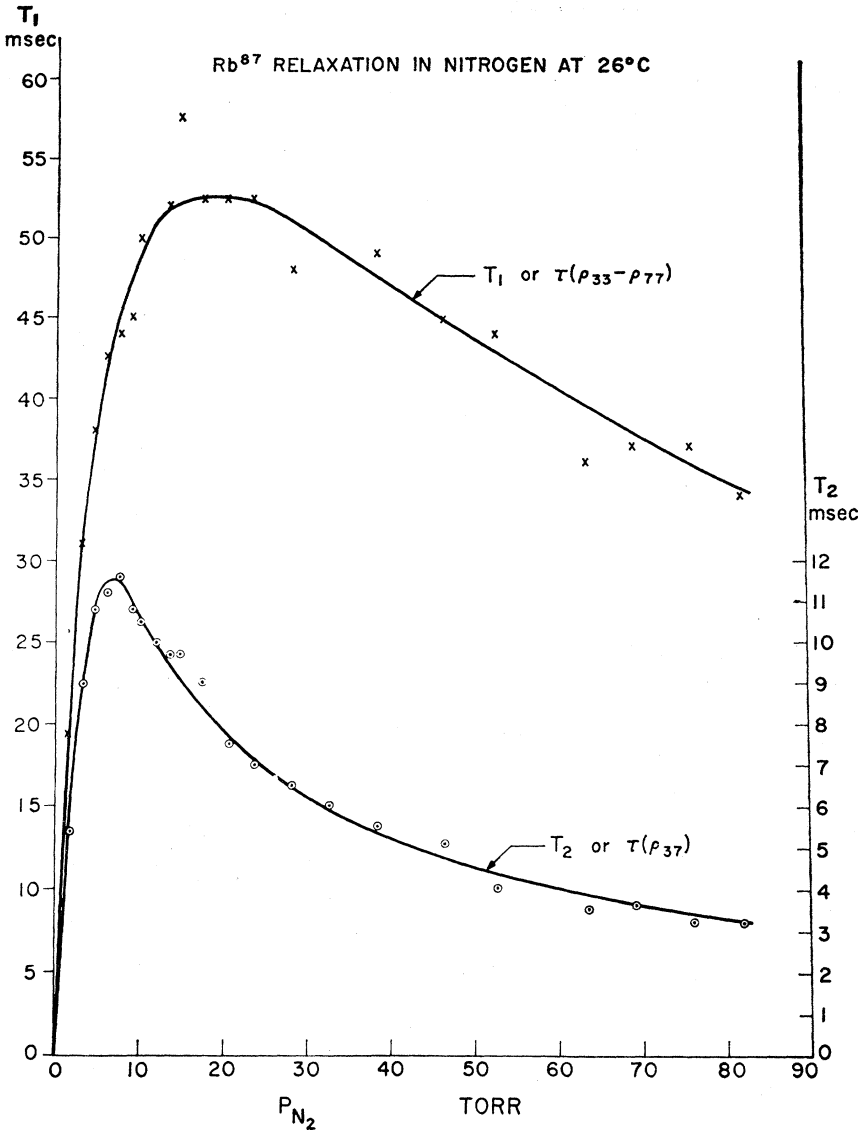

FIG. 7. Relaxation of Rb^{87} in nitrogen-14 as a buffer gas at room temperature.

to the buffer gas is approximately 100 msec. As pointed out by Franz,[26] impurities would affect the relaxation time even with a residual pressure of the order of 5×10^{-7} Torr. Assuming a cross section of about 10^{-14} cm^2 and a relative velocity of 5.5×10^4 cm/sec, Franz calculates the maximum value of T_1 to be 95 msec. Although the value assumed for the cross section appears somewhat arbitrary, it is of the order of magnitude of cross section found in spin-exchange interaction; the above calculations would show that at the residual pressure in our experiment (3×10^{-6} Torr), our longest relaxation times are affected by the presence of impurities. In that context, however, the decorrelation characteristic time T_2 would not be much affected by the presence of the residual impurities. This is because if spin exchange is the actual mechanism taking place between rubidium and these impurities, T_2 would then be of the order of magnitude of T_1. Consequently, due to the relatively low values measured for T_2, and long values for T_1, we do not expect to find T_2 affected much by this mechanism.

It should be mentioned that at the normal temperature of operation of the maser (60–70°C) spin-exchange interactions between rubidum atoms play a major role and the decorrelation of the buffer gas adds only a small contribution to the relaxation.

[26] F. A. Franz, University of Illinois Report No. R-246 (unpublished).

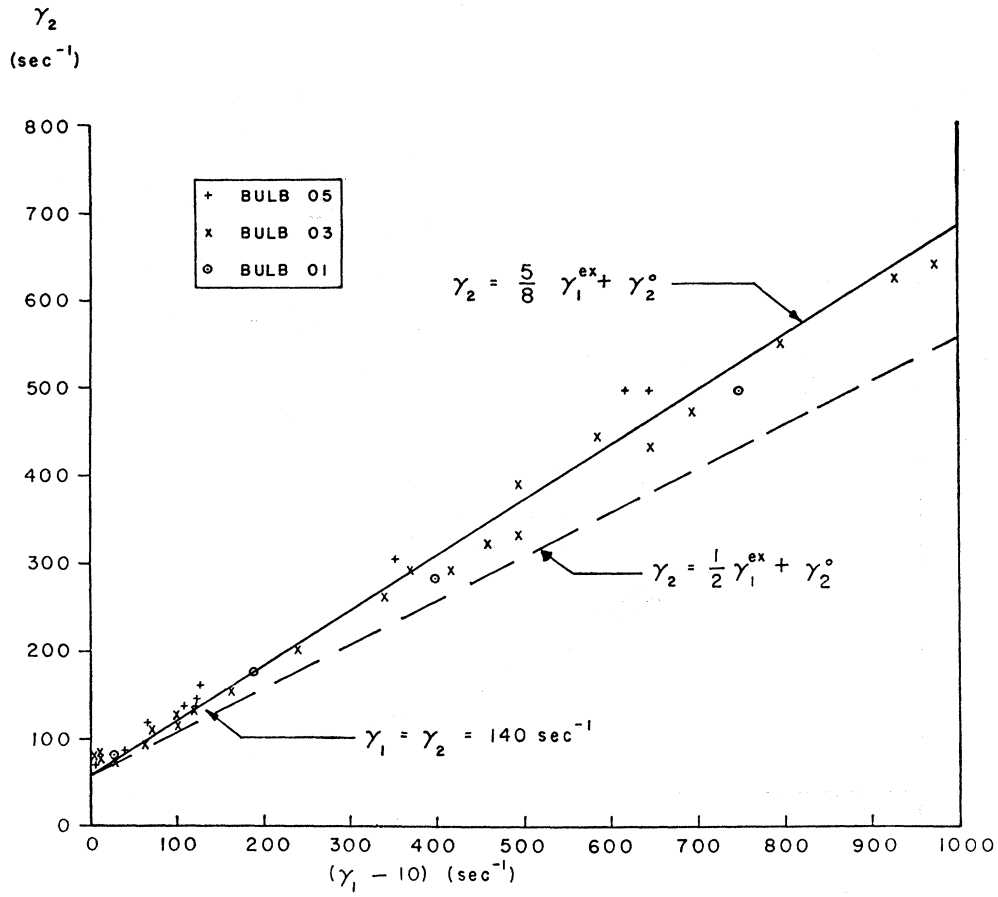

FIG. 8. Relaxation rate γ_2 plotted versus $(\gamma_1 - 10\ \text{sec}^{-1})$. The temperature is the variable; however, γ_1 as explained in the text, is used to measure the rubidium density. The solid line reflects the theoretical results obtained in an earlier section.

B. Rubidium-Rubidium Spin-Exchange Relaxation

The effect of spin-exchange interaction between rubidium atoms was determined as a function of temperature in nitrogen at a pressure of approximately 11 Torr. It was found, however, that the relaxation time T_1 measured depended very much on the history of the cell and on the physical location of the rubidium inside the cell. For example, the same relaxation time could be obtained in two different cells but at temperatures differing by as much as 10°C. Since, at moderate temperatures, the relaxation rate γ_1 is mostly controlled by spin-exchange interaction, the following procedure was found best in analyzing the data. First, a plot of γ_1 was made against the rubidium pressure as obtained from tables of vapor pressure versus temperature. Extrapolation to zero pressure gave an approximate value of the zero rubidium density relaxation rate. This value was approximately 10 sec^{-1} and was then subtracted from all the measurements of γ_1. From the results a graph of γ_2 versus $(\gamma_1 - 10\ \text{sec}^{-1})$ was made. This is shown in Fig. 8 for three bulbs, called 01, 03, and 05. The results for bulb 05 were obtained from a situation where optical pumping was accomplished from both ends of the cavity. In the case of bulb 03 a film of rubidium was present on the walls inside the bulb. The temperature needed to obtain a given γ_1 was approximately 10°C lower than in the other bulbs.

The solid line passed through the points in Fig. 8 is the line that would give

$$\gamma_1{}^{ex} = (8/5)\gamma_2{}^{ex}$$

as calculated in the theoretical section.[27] The dotted line would give $\gamma_1{}^{ex} = 2\gamma_2{}^{ex}$. The experimental results thus appear to confirm the calculation made earlier. There may be some question, however, about the high-density points. Since, at these high densities, the light gets absorbed closer to the ends of the cell and does not penetrate as far in the cell as in the case of lower density, the

[27] A least-squares fit of all the data points in Fig. 8 gave the following relation: $\gamma_2 = 63 + 0.61\gamma_1{}^{ex}$.

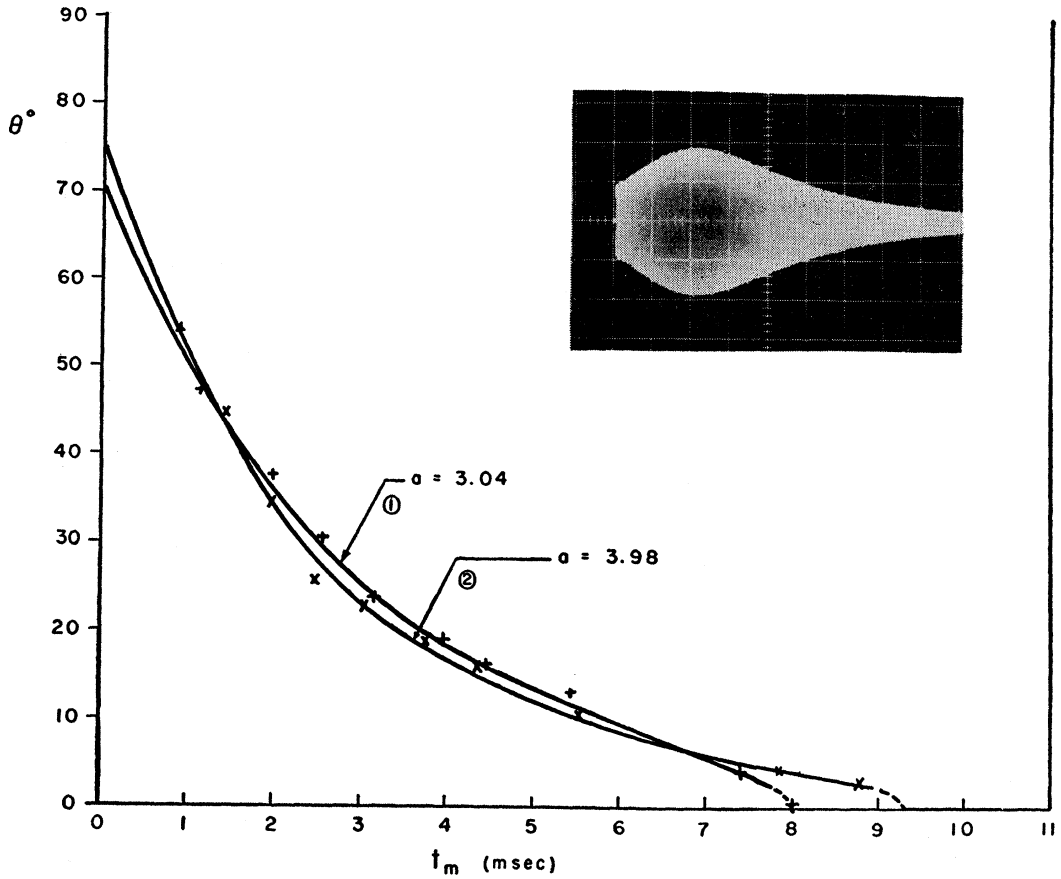

FIG. 9. A typical plot of the time at which power becomes maximum as a function of the rf pulse-driving phase angle θ_p. Curve (1) is for the case where one lamp only is used while curve (2) is for the case where the maser is pumped from both ends. The difference between these two curves comes from the difference in pumping rate. The insert is a typical photograph of a delayed power surge for $\theta_p \leq 90°$.

wall may start to play a more important role in the relaxation. However, the configuration of rf field is such that those atoms that contribute to the signal are not close to the ends of the cell. An interesting region on Fig. 8 is where γ_1 equals γ_2. This happens at a relaxation rate of about 140 sec^{-1}. This number depends on the buffer gas pressure since at low rubidium density γ_2 is primarily determined by buffer gas relaxation. The temperature at which this crossing region exists depends also very much on the history of the bulb. In one case where a rubidium film was present in the bulb, this point appeared at a temperature of 55°C. In another bulb where the rubidium was concentrated in the tip, the point was at 62°C.

The values of ($\gamma_1 - 10$ sec^{-1}) plotted on the abscissa in Fig. 8 can be used to determine the density in the following way. From the calculation made earlier, $\gamma_1^{ex} = n\bar{v}_r\sigma$ where n is the density, $\bar{v}_r$ is the relative velocity, and σ is the cross section. This last parameter has been determined by several experimenters.[28–34] As will be shown later, its value is approximately 1.6×10^{-14} cm^2. From this, and defining $\bar{v}_r = 4(kT/\pi m)^{1/2}$, one obtains $n = (\gamma_1/6.4)10^{10}$ holding approximately for the range of temperature used here.

C. Spin-Exchange Cross Section

In relaxation measurements as reported above, the effect of the rf magnetic field on the atoms themselves is

[28] H. Warren Moos and Richard H. Sands, Phys. Rev. **135**, A591 (1964).
[29] Hyatt Gibbs, thesis, University of California, Lawrence Radiation Laboratory, 1965 (unpublished); H. M. Gibbs and R. J. Hull, Phys. Rev. **153**, 132 (1967).
[30] S. M. Jarrett, Phys. Rev. **133**, A111 (1964).
[31] P. Franken, R. Sands, and J. Hobart, Phys. Rev. Letters **1**, 118 (1959).
[32] R. Novick and H. E. Peters, Phys. Rev. Letters **1**, 54 (1958).
[33] Marie Anne Boushiat, Étude par Pompage Optique de la Relaxation de Rubidium, Publications Scientifiques et Techniques du Ministère de l'Air, Paris (Service de Documentation et d'Information Technique de l'Aeronautique, Paris, 1965).
[34] S. M. Jarrett and P. A. Franken, J. Opt. Soc. Am. **55**, 1603 (1965).

assumed to be small. In other words, the radiation lifetime at the hyperfine frequency is assumed to be long compared to the relaxation time measured. In practice, this condition can be satisfied by increasing the cavity coupling and setting the cavity somewhat off resonance.

In the case where the radiation lifetime is of the same order of magnitude as the relaxation time, a delayed surge of power is observed some time t_M after the pulse. The physical explanation of the phenomenon is fundamental to maser action. It shows that after the spin system is sent into a radiant state, oscillation builds up to a point where the effect of relaxation takes over and makes the system decay to equilibrium. In a maser the relaxation is counteracted by replenishing the population of the upper energy level. In the present situation this does not happen since the orienting light is turned off during the time of observation of the effect.

The effect has been seen in the maser; its existence has been reported also by Bender and Driscoll in protons.[35] This effect was used to determine the spin-exchange cross section through the method described in the theory. The dependence of t_M versus θ_p obtained had the general form predicted by Eq. (48). This is shown in Fig. 9. There were, however, some slight discrepanices which were probably due to the difficulty of interpretation of θ_p. The driving phase angle θ_p of the pulse could be varied by changing either the pulse length or the rf amplitude. In changing the pulse length one had to be careful about the electronics response time. It was found in our case that below approximately 35 μsec, the pulse amplitude decreased with diminishing length. The other method of varying the pulse amplitude with a calibrated attenuator appeared to be more reliable.

The definition of the phase angle for a given pulse was somewhat ambiguous in our system. This was due to the fact that the rf field was not constant through the whole cavity. It was found that at exact resonance the power required for a 180° pulse was not exactly twice the power required for a 90° pulse. It appears that it would be desirable to make these experiments in a system where the atoms are confined to a field of approximately the same amplitude.

Even though there were some ambiguities like the ones described above, the effect was clearly observed and the results were analyzed in the following way. Either the pulse length or the field amplitude was varied. The signal amplitude immediately after the rf pulse was then recorded as well as the time of the maximum power after the pulse. The driving phase angle was obtained from the amplitude of the signal, and a plot of θ_p versus t_M was made.

Several methods were tried for extracting the parameter $a=\Delta_0 k/\gamma$ from the experimental data.

(1) One method consisted in trying various values of a to obtain the best fit between Eq. (48) and the experimental data. However, it was found that when this was done, Eq. (48) was not in agreement with the experimental data for large values of t_M when $\theta_p \to 0$. This was probably due to the ambiguity in defining the phase angle θ_p at intermediate values.

(2) Another method consisted in finding by extrapolation the value of θ_p for the case where $t_M \to 0$. Although this is a perfectly valid method, it was found rather difficult to use in practice because the relation between θ_p and t_M is not linear.

(3) A third method, which is probably the best one, was to use the value of t_M when $\theta_p \to 0$. In this case one can show from Eq. (48) that t_M tends to the value $\ln a/\gamma$, from which a can be obtained. This method has the advantage that it does not depend on the interpretation of θ_p at intermediate values.

The value of σ found through this last method near the temperature where $\gamma_1 \approx \gamma_2$ was

$$\sigma = 1.6 \times 10^{-14} \text{ cm}^2 \pm 0.3$$

and is in agreement with the best value published.[28,29] The error quoted here is the maximum scatter observed in the various measurements. This value of σ is approximately 20% smaller than the value published earlier, which was obtained through methods (1) and (2) described above.[10] The new value reflects the use of the third method of extracting the value of a from the experimental data, as well as new experiments that have been made since that time. Figure 9, which is a typical set of data, was obtained with bulb 05 and optical pumping either from both ends of the cavity or from one end only. The same value of σ was found for both cases, well within the experimental maximum error given above. The relative shape of the two curves is in agreement with the shape predicted by Eq. (48). However, Eq. (48) could not be fitted to the experimental data at both regions of intermediate θ_p and $\theta_p \to 0$ at the same time.

Several questions arise on the absolute accuracy of σ as determined here. The parameters Δ_0 and η could be inexact by a certain amount. To obtain σ, the value of η was first calculated for a bulb filling the entire cavity; this result was then multiplied by the ratio of the bulb volume to the cavity volume. The value of Δ_0 in general could be inexact due to two sources. First, an error in

[35] P. L. Bender and R. L. Driscoll, IRE Trans. Instr. **7**, 177 (1958).

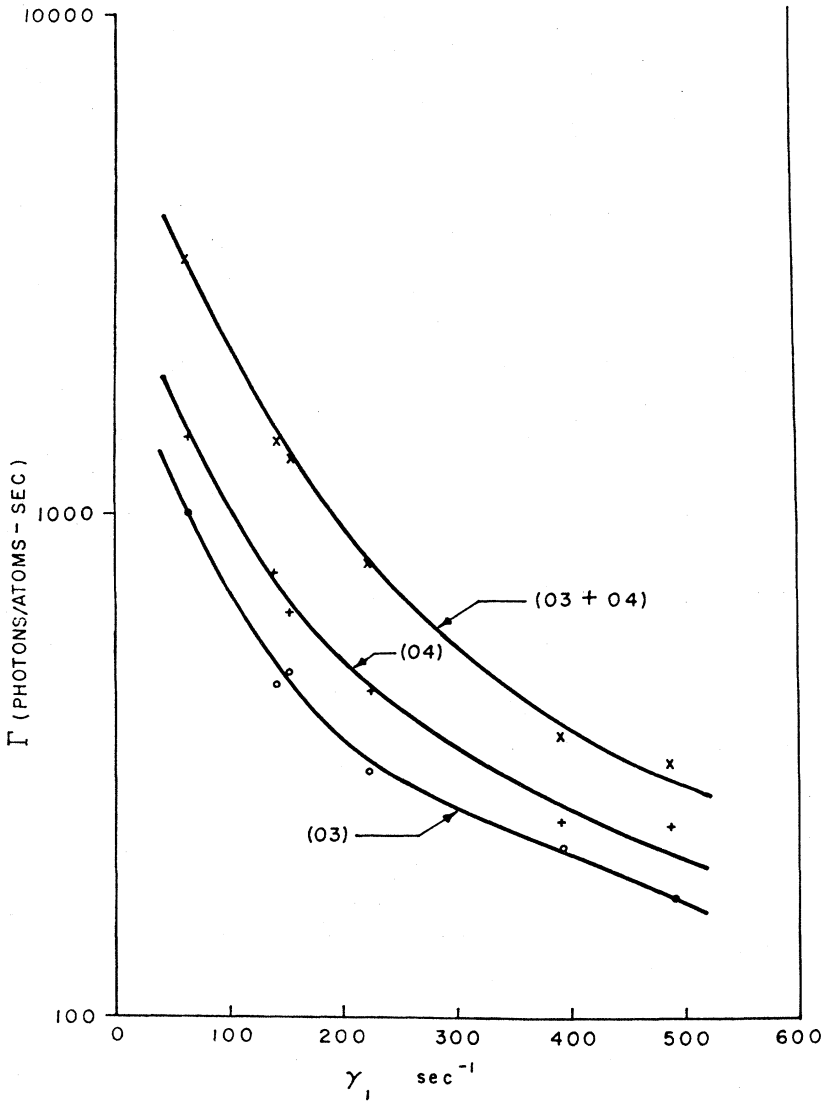

FIG. 10. Lamp pumping rates versus the maser relaxation rate γ_1.

the pumping rates could be reflected by an error on Δ_0. However, at the pumping rates used here, an error of 25% in Γ would be reflected by an error of only 7% in the value of Δ_0. The other source of error would be to some extent nonuniform illumination through the cell. However, it will be seen in the following section on pumping rates that the bulb is still relatively transparent at the density at which these experiments were done. The experimental data of Fig. 9 in which the bulb was optically pumped either from both ends or from only one end gave the same result as far as σ is concerned. The two lamps added to give a greater pumping rate without increasing the signal much as compared to the case where only one lamp was used.

The technique of determination of σ just described can be used in several other systems such as those using hydrogen, potassium, sodium, rubidium-85, and cesium. In each case a different method would be used to obtain the orientation.

D. Pumping Rates of Lamps and Maser Power Output

The pumping rates of the lamps were determined by the method shown in Fig. 4 in a bulb filled with nitrogen at a pressure of 11 Torr. At the turn-on of the light, orientation starts in the spin system. Orientation takes place within a characteristic time which is a measure of the pumping rate of the lamp and of the relaxation rate γ_1. This characteristic time is $(\frac{5}{8}\Gamma+\gamma_1)^{-1}$. It is measured by monitoring with a 90° pulse the amount of orientation obtained at a given time after the light has been turned

on. This has been done on a maser equipped with two lamps—one at each end; the pumping rate of either lamp individually or of both lamps acting together has been measured as a function of the density (or γ_1) in the maser cell. These lamps are called 03 and 04, respectively, and the results are shown in Fig. 10.

The variation of the pumping rate Γ with density and distance in the absorption cell can be estimated in the following way. We assume a spectrum having a rectangular line shape of width equal to the Doppler width and around the wavelength corresponding to the transition $P \leftrightarrow S(F=1)$. The absorption line in the maser cell is assumed to have the same shape and the same width. Although these are crude assumptions, the result obtained is sufficient to explain qualitatively the experimental behavior of the pumping rate Γ. We define σ_0 as the absorption cross section for the absorption of an incident photon by a rubidium atom. Taking into account the effect of the light in increasing the cell transparency we obtain the following relation:

$$(8/3)\gamma_1 \ln(\Gamma/\Gamma_0)+(5/3)(\Gamma-\Gamma_0)=-(\sigma_0/\sigma v_r)\gamma_1^2 z, \quad (57)$$

where z is the distance in the cell and where we have used the relation $\gamma_1 \simeq n\bar{v}_r\sigma$.

The experimental results shown in Fig. 10 reflect qualitatively the behavior predicted by Eq. (57). The large rate of decrease of Γ observed at low values of γ_1 is in agreement with the prediction that the pumping rate should decrease with the square of the density.[36] At higher density the observed rate of decrease of Γ with density is less than at lower density. This would show that the logarithmic term in Eq. (9) is becoming important relative to the linear term in Γ. In this case Γ would decrease exponentially with γ_1. When the experimental values are entered into Eq. (9) and z is taken as one-half the length of the cell, a value of σ_0 of the order of 2×10^{-11} cm^2 is obtained. This is of the order of magnitude known for the absorption cross section for rubidium resonance radiation. Detailed comparison of the experimental data with the theory, however, shows that Eq. (57) predicts a faster decrease of Γ with density than the one observed. This is probably because at these higher densities, the center of the rubidium line is absorbed and much of the pumping is done by the wings of the line. In that case the cross section for absorption of photons in the wings of the line is small; this would predict a less rapid decrease of the intensity with the density. This effect was not included in Eq. (57) since the cross section σ_0 was assumed constant through the absorption line of width equal to the Doppler width.

In Fig. 11 the ratio $\Gamma(03+04)/(\Gamma03+\Gamma04)$ is plotted. It is seen that this ratio drops monotonically with increasing cell density, showing that the region of interaction of the lamps is becoming more separated at the higher temperatures. However, at the temperature of operation of the maser where $\gamma_1 \sim 300$ sec^{-1}, one can see that both lamps are still interacting at overlapping regions of space. At low densities both lamps help each other by making the cell more transparent and allowing the light to penetrate the region of space where the rf field has the proper orientation.

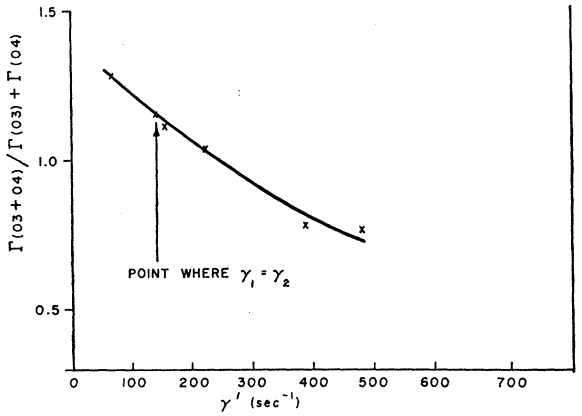

FIG. 11. Plot of the ratio of the pumping rates of both lamps acting together, to the sum of the pumping rate of each lamp acting separately. The result shows that the overlap of the region of interaction of the lamps decreases with increasing density.

The maser power output was studied under cw operation as a function of various parameters such as cavity Q, density, and light intensity. In the first experiment the bulb was filled with 11 Torr of nitrogen and 10 mg of Rb^{87}. The maser in which these measurements were made had a transparent top tuner and a solid bottom which probably had a certain amount of reflectivity at the wavelength of the pumping light. Only one lamp was used in these experiments.

The light intensity was varied by the means of an iris in front of the light beam. Light pipes were used in the experiment and it is beleived that redistribution of intensity in the beam was not appreciable when the light intensity was varied through that technique. The pumping rate of the lamp was measured by the method described earlier; this was done for various iris settings and various densities in the maser. The lamp and filter cell temperatures were adjusted to give optimum performance.

Using these measurements it was possible to make graphs of the maser power output as a function of light intensity for various parameters and cavity Q values. The cavity Q was varied by changing the amount of coupling. The original data of power output has been transformed to an actual power given by the atomic system and it is this power that is plotted in Fig. 12. These two powers are related by

$$P_{\text{out}}=P\times k_c/(1+k_c), \quad (58)$$

[36] At low values of γ_1, Γ is close to Γ_0, the value of Γ when γ_1 tends to zero.

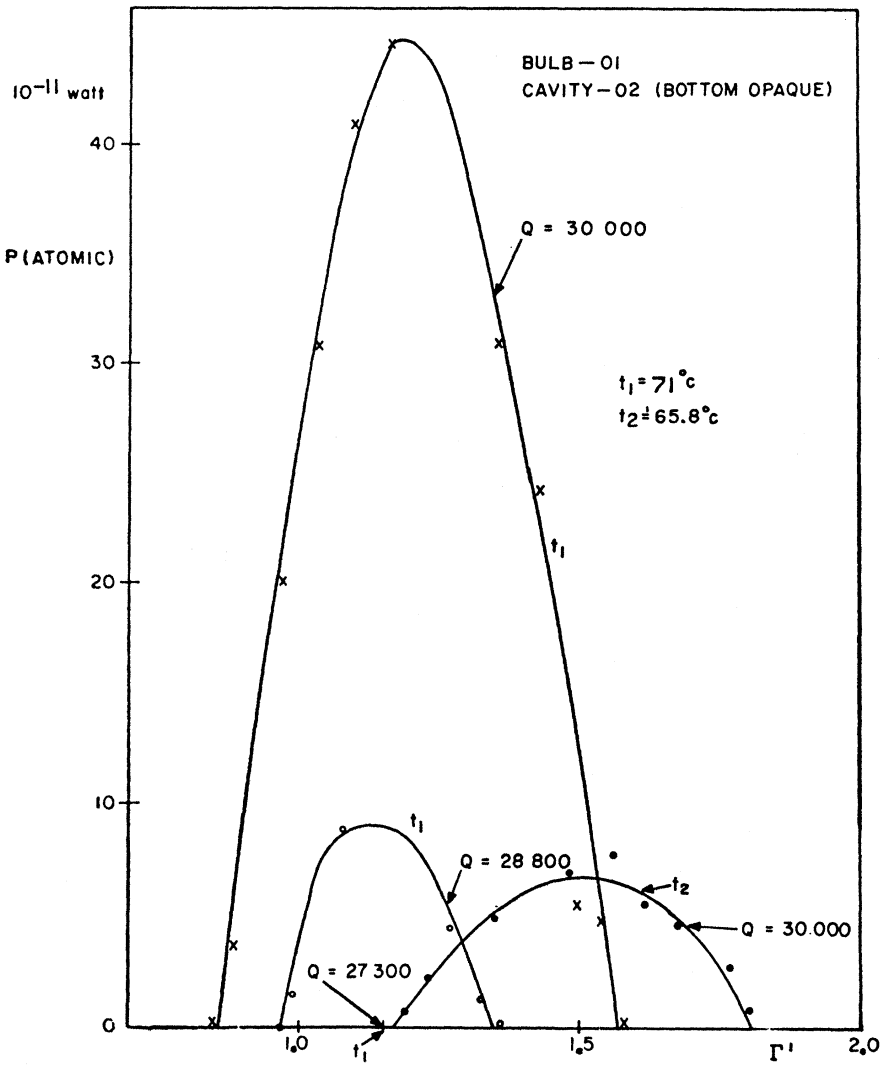

FIG. 12. Power output of the rubidium maser versus light intensity for various values of the maser parameters.

where k_c is the coupling coefficient for an undercoupled cavity.

These results follow the general characteristic of the theory described earlier. However, there are some marked differences:

(1) The range of $\Gamma'=\Gamma/\gamma_1$ over which the maser operates is very narrow. From the value of $\Delta_0 k/\gamma$ obtained earlier, the parameter Γ_m' can be evaluated through the relation $\Gamma_m'=\gamma/k$. The value found is about 0.04 which, from Fig. 3, would permit a range of oscillation from $\Gamma'=0.6$ to $\Gamma'\approx 6$. This is not seen in Fig. 12.

(2) When the density in the maser cell is raised, the maximum of power appears to move toward lower values of Γ'.

The reason for this behavior is not yet completely understood. However, one can mention the presence of the following effects. If the buffer gas is not quenching all the scattered radiation, there will be trapped radiation and a loss of orientation at high light intensity; this could reduce the range of operation of the maser as a function of light intensity. Another effect is the modulation of the light by the oscillating atoms.[37] This would introduce side bands in the lamp spectrum; one of these side bands would appear at the resonance wavelength connecting the P state to the $F=2$ level in the ground state. This would destroy the spin orientation in the maser and lower the power output. In the experiments reported here a maximum power of 2×10^{-10} W has been observed for the case where the maser oscillates between the field-independent levels. In zero field where all the Zeeman levels are overlapping, a power output of 10^{-9} W was detected.

[37] R. Novick (private communication).

V. CONCLUSIONS

From the results reported here it can be concluded that the theory underlying the operation of the rubidium maser is fundamentally in agreement with the experimental data. However, there are some discrepancies between the theory and the experimental results which are not yet understood. From the results of measurements on the power output of the maser, it appears that the rubidium maser should be a source of unsurpassed spectral purity.

In this paper the theory of spin-exchange interaction between Rb^{87} atoms has been developed and has been found in agreement with the experimental data. Experiments have also been described in which the spin-exchange cross section has been measured through a new method utilizing stimulated emission. The result has been found in agreement with the data published. The method should be extended to other systems such as those using sodium, potassium, cesium, and rubidium-85.

ACKNOWLEDGMENTS

The writer wishes to thank Dr. A. O. McCoubrey for his encouragement throughout the course of this work. Thanks also are expressed to Dr. R. F. Lacey, Professor R. Novick, Professor W. Happer, Dr. J. Holloway, Dr. R. F. C. Vessot, and Dr. M. Baker for many stimulating discussions. The writer also wishes to thank R. F. C. Vessot, Dr. M. Baker, and Dr. L. Cutler for many stimulating discussions. The writer also wishes to thank his wife Lucie for her help in calculating spin-exchange matrices and Peter Cato who constructed most of the apparatus. Thanks are also due to Dr. P. Bender for suggestions on the manuscript.

This work has been supported by the U. S. Army Electronics Command, Fort Monmouth, N. J., and the National Aeronautics and Space Administration, Goddard Space Flight Center, Greenbelt, Md.

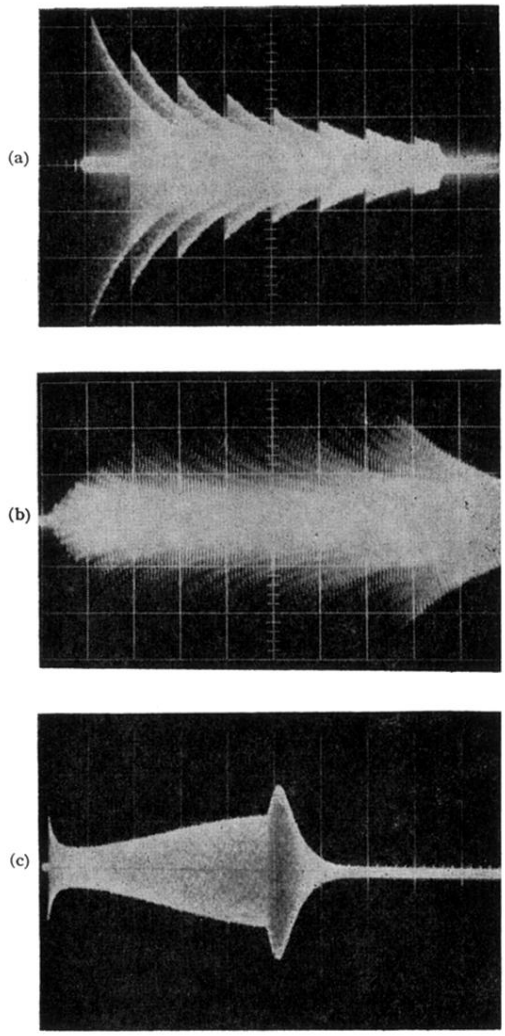

FIG. 5. Typical experimental results. Photograph (a) shows a multiple exposure of the induced signal after the microwave pulse. The time base is 10 msec/div and the trace is triggered by the end of the light pulse. Photograph (b) is a multiple exposure of the growth of the orientation during the light pulse; in that case the trace is triggered from the beginning of the light pulse. The time base is 1 msec/div. In photograph (c), the maser gain is sufficiently high to permit continuous oscillation. The time base is 10 msec/div and the scope is triggered from the beginning of the light pulse. The light pulse ends at about 48 msec where the power output rises because the decorrelation effect of the light is removed.

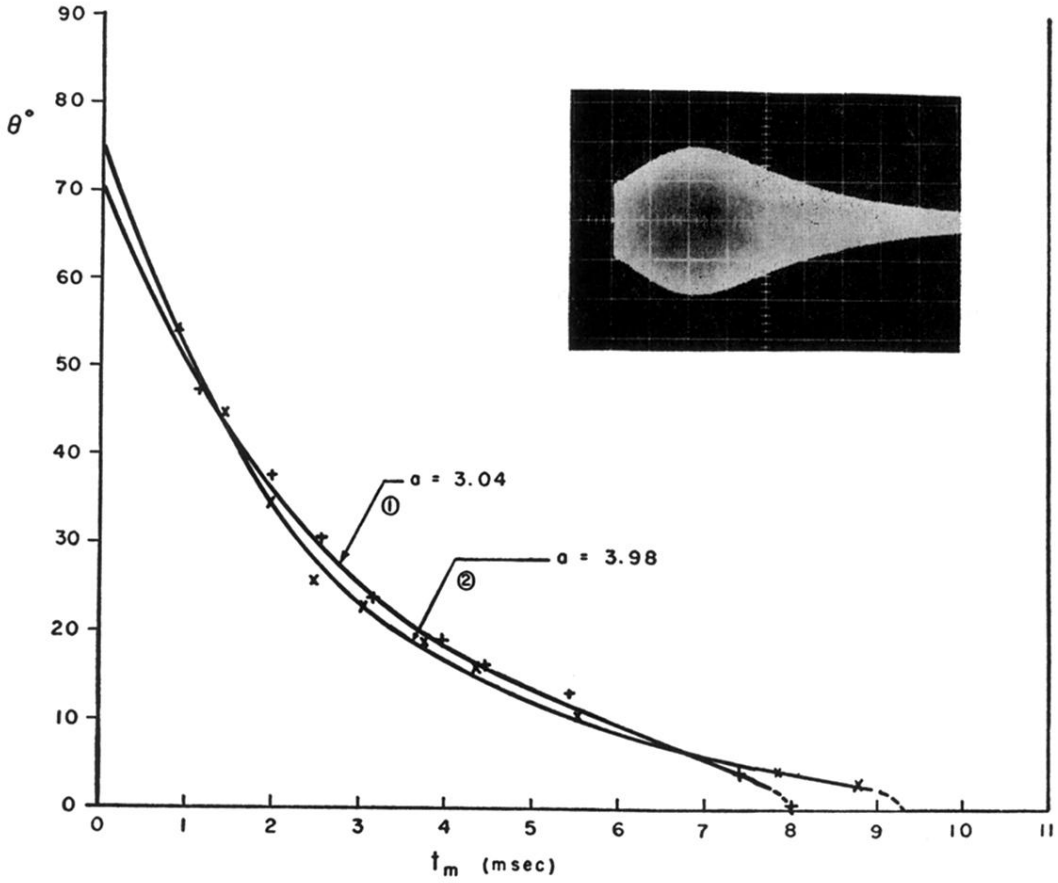

FIG. 9. A typical plot of the time at which power becomes maximum as a function of the rf pulse-driving phase angle θ_p. Curve (1) is for the case where one lamp only is used while curve (2) is for the case where the maser is pumped from both ends. The difference between these two curves comes from the difference in pumping rate. The insert is a typical photograph of a delayed power surge for $\theta_p \leq 90°$.